Last Glacial Maximum extent and subsequent retreat of the East Antarctic Ice Sheet from the Mac. Robertson Shelf

Janina Güntzel[1,2], Juliane Müller[1,3], Ralf Tiedemann[1,2], Gesine Mollenhauer[1,2,3], Lester Lembke-Jene[1], Estella Weigelt[1], Lasse Schopen[2], Niklas Wesch[2], Laura Kattein[1], Andrew N. Mackintosh[4] and Johann P. Klages[1,3]

[1]Department of Geosciences, Alfred Wegener Institute Helmholtz Centre for Polar and Marine Research, Bremerhaven, Germany
[2]Department of Geosciences, University of Bremen, Bremen, Germany
[3]Cluster of Excellence "The Ocean Floor – Earth's Uncharted Interface", University of Bremen, Germany
[4]Securing Antarctica's Environmental Future, School of Earth, Atmosphere and Environment, Monash University, Clayton, Victoria, Australia.

Correspondence to: Janina Güntzel (janina.guentzel@awi.de)

Abstract. The future behavior of the Antarctic Ice Sheet is considered to be one of the largest uncertainties in global climate projections, with its stability fundamentally governed by grounding zone processes, bed geometry, and sensitivity to oceanic forcing. However, observational records only reflect a short moment, when considering the length of a full cycle of ice sheet expansion and retreat. Therefore, paleo-data present a valuable extension to the observational period. East Antarctica's deglaciation history remains largely understudied compared to the West Antarctic margin. This emphasizes the urgent need for reliable long-term spatiotemporal data on ice sheet change, particularly for sectors that play key roles in supplying the world's oceans with dense bottom water. In this study, we performed a multi-proxy analysis on geophysical and geological data recovered from two prominent glacial cross-shelf troughs on the Mac. Robertson continental shelf. We classified submarine glacial landforms on the continental shelf along both troughs from combined multibeam swath bathymetry and sub-bottom profiler data to infer past grounding line extent and the pattern of subsequent grounding line retreat. Additionally, combined sedimentological, sediment-physical, and geochemical analyses, including foraminifer radiocarbon dating, reveal the style and timing of this retreat across the shelf. Our study concludes that grounded ice reached the Mac. Robertson continental shelf break until just before ~12.7 cal. ka BP, hence preventing the formation of Dense Shelf Water (DSW) in its current form. We therefore infer a different formation mechanism for DSW as an important precursor of Antarctic Bottom Water under such full glacial conditions before continued grounding line retreat exposed the middle continental shelf by ~10.8 cal. ka BP and set the stage for more modern-like conditions.

1 Introduction

The East Antarctic Ice Sheet (EAIS) is the largest ice sheet on Earth and is, in contrast to the West Antarctic Ice Sheet (WAIS), mostly situated above sea level. Ice mass loss has accelerated significantly over the last decades, driven by drainage from ice streams and outlet glaciers from the interior toward the ocean (e.g., Rignot et al., 2011; Fretwell et al., 2013), with dominant losses from West Antarctica (e.g., Rignot et al., 2019). However, the cumulative contribution to sea level rise from the EAIS is assumed to have recently caught up with that from the WAIS (e.g., Rignot et al., 2019; The IMBIE Team, 2018). While large-scale differences in ice sheet geometry largely explain contrasting stability between the EAIS and WAIS, the ultimate expression of this instability is governed by processes operating at the grounding zone. Regions located on retrograde slopes and/or in submarine basins with elevations below sea level are particularly prone to grounding line instability (Weertman et al., 1974; Schoof et al., 2007). Many parts of the EAIS show a significantly different bed topography on the continental shelf and underneath the ice sheet (Pritchard et al., 2025). Due to the different bed characteristics, individual regions may react very differently to external forcings such as the inflow of relatively warm Circumpolar Deep Water (CDW), today, but also likely throughout the geological past (cf., Mawbey et al., 2026). The extent of grounded ice on the continental shelf not only reflects ice sheet dynamics but also directly influences shelf-water formation processes and ocean circulation (e.g., Silvano et al., 2016). However, for most sectors along the EAIS margin, reliable data about past grounding line (GL) extent and subsequent retreat is either highly fragmentary or entirely missing (Mackintosh et al., 2014) and preventing a proper assessment of past AIS size variability with its potential effects on, e.g., sea level rise and/or ocean circulation changes (e.g., Bradley and Hewitt, 2024). Previous work by the RAISED Consortium (2014) suggests that the EAIS likely extended towards outer continental shelf regions during the Last Glacial Maximum (LGM) and retreated to or near modern positions by ~5 cal. ka BP, but data about the last deglaciation remain sparse. As a result, targeted regional studies are required to solve the timing of the grounding line retreat and its implications for ice-ocean interactions.

We investigated the spatiotemporal extent and subsequent retreat of the GL across the Mac. Robertson continental shelf, where dense shelf water (DSW) currently forms due to brine rejection from sea ice formation in coastal polynyas, eventually contributing 20-25% of Antarctic Bottom Water (AABW) (e.g., Wong and Riser, 2013; Schmidt et al., 2023; Mizuta et al., 2024). This makes it highly relevant to reliably assess whether the continental shelf was covered by grounded ice during the LGM and thereafter, i.e., if DSW formed there via the modern formation mechanism, with direct implications for better characterizing circum-Antarctic Ocean circulation during past glacial maxima.

We present a multi-proxy approach on geophysical and geological data, including numerous sediment cores from two major cross-shelf glacial troughs, Nielsen Basin and Iceberg Alley. From this, we identify the maximum ice sheet extent, initial GL retreat, and the pattern of its subsequent retreat. Previously, the timing of deglaciation for the Mac. Robertson continental shelf after the LGM was assumed to have been initiated between 14.0 and 12.0 cal. ka BP, but it remained uncertain whether or not the GL reached the continental shelf break (Leventer et al., 2006; Mackintosh et al., 2007; Mackintosh et al., 2011). We introduce a comprehensive, four-dimensional framework for the timing of initial GL retreat after the Last Glacial Maximum

(~26-19 ka BP) and provide new evidence for a GL that reached the Mac. Robertson continental shelf break, implying absent DSW formation in its current form, with direct implications for AABW production.

2 Study area

The continental shelf offshore the Mac. Robertson Land is relatively narrow (<90 km width) and comprises shallow banks that are cut by deeper cross-shelf troughs. It is bordered by the Amery Ice Shelf towards the East and the Kemp Land and Enderby Land to the West (Fig. 1) and is characterized by a shallower outer shelf (~300-500 m), a general deepening towards the inner shelf, with overdeepened cross-shelf troughs reaching the shelf break (Fig. 2). The prevailing currents in the area are the Antarctic Coastal Current (ACoC), which rotates counter-clockwise along the coast around Antarctica (Fig. 1). Other important ocean currents on the continental shelf and at the shelf break are the Antarctic Slope Current (ASC), which can drive Circumpolar Deep Water onto the continental shelf and Dense Shelf Water (DSW) formation, which is formed in seasonal polynyas. The Cape Darnley Bottom Water (CDBW), a precursor of AABW, is produced in the Cape Darnley polynya, which is located offshore Cape Darnley (Oshima et al. 2013; Mizuta et al. 2024) on the easternmost Mac. Robertson continental shelf (Fig. 1). This alters the formation of fresher DSW in front of the ice shelf. The CDBW then flows down the continental slope, mixing with CDW by brine rejection in sea ice-free areas, eventually contributing to westward-flowing AABW (Oshima et al., 2013).

The most prominent geomorphic features on the Mac. Robertson continental shelf are two cross-shelf glacial troughs, the Nielsen Basin and Iceberg Alley, that likely acted as major corridors for fast-flowing ice streams during the last glacial (Leventer et al., 2006; Mackintosh et al., 2011). The Nielsen Basin is more sinuous in shape with a maximum water depth of ~1,300 m (Iceberg Alley: ~850 m) but both troughs are characterized by a reverse bed slope, i.e., deepening landwards (Leventer et al., 2006; Fig. 2). Previously, two minor grounding zone wedges have been identified on the outer shelves of Nielsen Basin and Iceberg Alley (Mackintosh et al., 2011), which we refer to as “GZW-I” and “GZW-II” (Fig. 2). These GZWs, which, in both troughs, occur at similar water depths (~390 mbsl), were suggested to indicate maximum GL advance in Nielsen Basin and Iceberg Alley during the LGM (Mackintosh et al., 2011; Fig. 2).

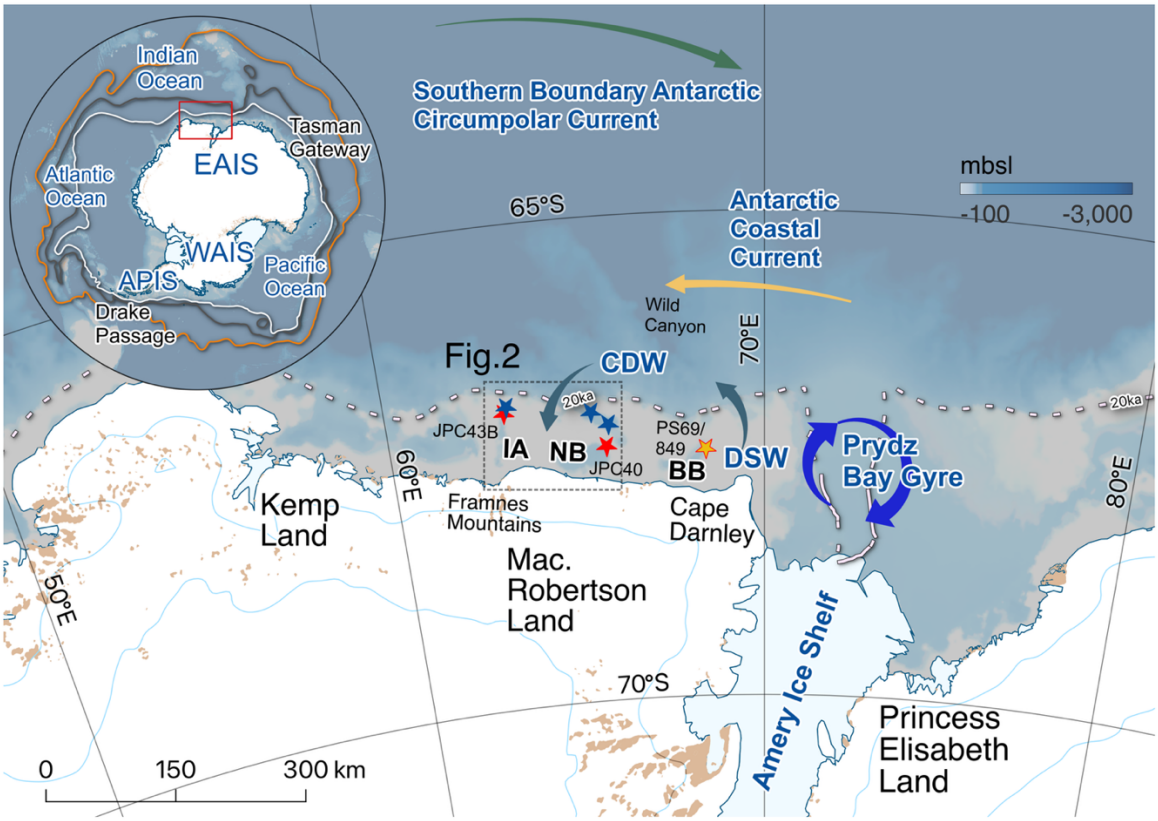

Figure 1: Overview of the study area. Polar Front (PF; orange), southern Antarctic Circumpolar Current Front (ACCF; green), and Antarctic Circumpolar Current (ACC; white) are indicated in the upper left panel. Clusters of sediment cores investigated for this study from the Nielsen Basin (NB) and Iceberg Alley (IA) are indicated by the blue stars (cf. Fig. 2). Existing cores used for this study are marked by red (IA, NB) and yellow stars (BB), respectively. The dotted line represents the inferred grounding line position at the LGM (The RAISED Consortium, 2014). Arrows indicate the flow direction of major ocean currents in the area. IBCSO v2 (Dorschel et al., 2022) modified with Quantarctica package for QGIS (Matsuoka et al., 2021).

3 Materials and methods

The eight sediment cores analyzed for this study were retrieved from the mid–outer Mac. Robertson continental shelf during the R/V *Polarstern* (AWI, 2017) Expedition PS128 "East Antarctic Ice Sheet Instabilities" (EASI-I) (Tiedemann and Müller, 2022) in the Austral summer of 2022. Most cores were recovered with a Kiel-type gravity corer (GC), while at sites PS128_38 and 39, a piston corer (PC) was used (Table 1). Physical properties of the sediments were measured onboard with a GEOTEK Multi Sensor Core Logger (MSCL), and stored at + 4 °C. Visual core descriptions, documentation, and sampling were performed at the Alfred Wegener Institute (AWI) in Bremerhaven, Germany.

Geophysical data (multibeam swath bathymetry and sediment echography) were collected simultaneously on Expedition PS128, and combined with existing data from *Nathaniel B. Palmer* Expedition NBP0101 in 2001 (Leventer et al., 2006;

Mackintosh et al., 2011) to identify glacial bedform assemblages along the mid–outer continental shelf in Nielsen Basin and Iceberg Alley (Fig. 2).

Table 1: Sediment cores analyzed for this study. GC: Gravity corer; PC. Piston corer; deg: Decimal degree; mbsl: meters below sea level; mbsf: meters below sea floor; GZW: Grounding-zone wedge.

Core Nr.	Device	Latitude (deg)	Longitude (deg)	Water depth (mbsl)	Core recovery (mbsf)	Location
PS128_45-1	**GC**	-66.952	64.858	356.8	1.29	Outer shelf, Nielsen Basin
PS128_44-1	**GC**	-66.960	64.990	399.8	3.96	Outer shelf, Nielsen Basin
PS128_42-1	**GC**	-67.067	65.498	580.7	4.07	Mid shelf, Nielsen Basin, GZW
PS128_41-1	**GC**	-67.092	65.600	584.4	4.06	Mid shelf, Nielsen Basin, GZW
PS128_39-1	**PC**	-67.115	65.696	660.6	8.60	Mid shelf, Nielsen Basin, sedimentary basin
PS128_38-2	**PC**	-67.142	65.817	524.6	0.77	Mid shelf, Nielsen Basin
PS128_46-1	**GC**	-66.843	63.188	376.1	2.62	Outer shelf, Iceberg Alley, GZW
PS128_47-1	**GC**	-66.828	63.208	389.8	3.92	Outer shelf, Iceberg Alley

3.1 Geophysical analyses of the (sub) seafloor

The bathymetric data from Expedition PS128 were acquired with the multibeam echosounder (MBES) Teledyne Reson Hydrosweep DS3 with a frequency of ~14 kHz in chirped pulses, arranged in a Mills Cross configuration of 3 x 3 m. The bathymetric data from NBP0101 were acquired with the SEABEAM system (Leventer et al., 2006). Both the PS128 and NBP0101 data were processed with the MB-system and spatially gridded with 25 x 25 m and 50 x 50 m, respectively, for further analysis with QGIS.

Sub-bottom profiles were acquired with the hull-mounted Deep-Sea Sediment Echo Sounder System PARASOUND P70 (Teledyne Reson, Bremen, Germany). For the expedition setting, two high-frequency acoustic signals of 18 and 22 kHz were transmitted, generating a low-frequency signal of 4 kHz in the water column. In our study, this low-frequency signal penetrated the sediment column to a depth of about 50 m and with a vertical resolution of about 30 cm to image the upper tens of meters of the subsurface on formerly glaciated shelves. This largely depends on the sediment's degree of stiffness (e.g., Klages et al., 2017; Arndt et al., 2017). The combined acoustic signal has a beam width of ~4 °. The resulting beam's footprint and thus the horizontal resolution on the seabed is about 7 % of the water depth.

3.2 Multi-proxy analyses of sediment cores and radiocarbon dating

Before sampling the cores, all sections were X-rayed either with computed tomography (CT) or by scanning 1 cm-thick sediment slabs at the AWI in Bremerhaven. The standard sampling interval for shear strength measurements and further sample

analyses was usually set to 10 cm, but guided by lithological or structural changes. Smear slides were taken from each identified lithological unit to support visual core descriptions and to further define microfossil content and composition. Magnetic susceptibility has already been determined onboard R/V *Polarstern* with a GEOTEK multi-sensor core logger. Syringe samples (10 cubic centimeters; cc) were removed, wet-weighed, freeze-dried, ground, and dry-weighed to determine water content and geochemical parameters such as total organic carbon (TOC) and nitrogen (N) content. For TOC, inorganic carbon – including carbonates – has been removed from 0.1 g of sediment with hydrochloric acid (20 % HCL) before the samples were measured with an ELTRA CS800 carbon-sulfur determinator (error ± 0.02 %). Total C and N contents of the bulk sediment were obtained with a Vario cube organic elemental analyzer by high-temperature combustion (error C, N ± 0.02 %). The ratio of carbon to nitrogen (C:N) was calculated from TOC/N_{tot} (%).

Spatula samples (~30 cc) from identical depths were sieved for grain size classification after freeze-drying with > 2 mm and > 63 μm-meshed sieves, respectively. The weight percentages were calculated from the total dry weight of the sample and the resulting weight of the dried grain size fractions, i.e., gravel (> 2 mm), sand (> 63 μm), and mud (< 63 μm), with water content calculated by subtracting the total dry weight from the wet weight. Sufficient amounts of calcareous microfossils were extracted for AMS ^{14}C dating from outer (PS128_44-1, 45-1, PS128_46-1, and PS128_47-1) and mid-shelf core PS128_39-1 (Table 3 and Supplementary Table S1). Before microfossil extraction, each depth was closely investigated on X-radiographs to exclude iceberg and/or bioturbation, potentially leading to unreliable measurements. Extracted foraminifer assemblages mainly included planktic species in core PS128_45-1 and benthic species in the cores PS128_39-1, PS128_44-1, PS128_46-1, and PS128_47-1. Even though calcareous microfossils are poorly preserved in continental shelf sediments (Hauck et al., 2012) as they are often bathed in corrosive Southern Ocean deep waters that currently spill onto shelves in many regions around the continent (e.g., Lanham et al., 2025), they provide the most reliable ^{14}C age control for Antarctic shelf sediments deposited during the last ~40 ka (e.g., Klages et al., 2017; Mawbey et al., 2026). For the present work, AMS ^{14}C dating was carried out with the MIni CArbon Dating System (MICADAS) on planktic and benthic calcareous microfossils at the Alfred Wegener Institute, Bremerhaven, Germany, following established workflows (Mollenhauer et al., 2021).

For core PS128_39-1, we additionally applied Ramped-Pyrolysis-Oxidation (RPO) ^{14}C dating to improve the age constraint for the alternating diatomaceous oozes in the upper part of the core. For that, we used a modified SoliTOC Cube Carbon Analyzer (Elementar Analysensysteme GmbH, Germany), also located at the MICADAS facility. Based on the shape of the thermograms (evolved CO_2 over temperature), the temperature limit for an appropriate fraction was determined such that the upper temperature limit was as low as possible while including a total amount of 80-100 μgC (Mollenhauer et al., 2021; Kattein et al., in rev.; cf. Supplementary Table S1). To ensure comparability to other Antarctic shelf sediment records, we corrected all ^{14}C ages by subtracting the marine reservoir effect for Antarctic shelf sediments (1300±100 ^{14}C years; Berkman and Forman, 1996; Ingolfsson et al., 1998; Anderson et al., 2002). We then calibrated the ages with the CALIB 8.2 software (Stuiver and Reimer, 1993), including the Marine20 calibration curve (Heaton et al., 2020), also considering their approach for Antarctic Holocene samples younger and older than 11.5 cal. ka BP (Heaton et al., 2023). To ensure comparability to previously dated

sediment cores in the region, we recalibrated published ^{14}C ages from JPC40 and JPC43B (Leventer et al., 2006) and PS69/849-2 (Borchers et al., 2016).

4 Results

4.1 Seafloor geomorphology and sub-seafloor stratigraphy

Identifying submarine glacial landforms that can be clearly linked to the former presence of ice gives us information about the past ice sheet's grounding line position, dynamics, and retreat styles, which is possible because many of these landforms are well preserved on the seafloor (Wellner et al., 2006; Dowdeswell et al., 2016).

Submarine glacial landform assemblages in the study area can be grouped into three classes: 1) Elongated, streamlined, and/or (sub)parallel, 2) wedge-like, and 3) randomly oriented curvilinear features. In the Nielsen Basin, we defined a distinct bedrock sill (elevated by ~150 m relative to the surrounding topography) that separates the deeper inner-shelf part of the trough from the mid-shelf. Adjacent to the sill, deeper basins characterized by clusters of (sub)parallel and elongated ridges with elongation ratios >10:1 are present. Towards the sill's top, those ridges transition into teardrop-shaped features before becoming more elongated again in seaward direction (elongation ratios >20:1; Fig. 3; b). Towards the top of the sill, sediment cover thins out, whereas it significantly thickens towards the center of adjacent basins (Fig. 3; profile A-A'). In the mid-shelf Nielsen Basin, several wedge-shaped (steep distal and gentle proximal slope) ~1 km long and ~8 m high bathymetric features are located perpendicular to the trough axis. Their internal composition appears largely transparent to chaotic on sub-bottom profiles (Fig. 3; profile X-X'). At the mid–outer shelf transition, the seafloor shallows significantly from ~500 to ~300 mbsl (Fig. 2a; vertical cross-section c). Here, the sets of elongated, streamlined features become increasingly overprinted by randomly oriented curvilinear structures, which are characterized by a general NNW-orientation.

On the outer shelf, randomly oriented curvilinear features comprise the entire area with highly variable orientations and depths. The presumed LGM GZW-II (cf. Mackintosh et al., 2011; Fig. 2a and cross-section panel c), lies in water depths of ~390 mbsl with a crest height of ~10 m and an along-flow length of ~6 km. Seaward from GZW-II, several multidirectional curvilinear features with ~5 to 10 m depths and with up to 200 m widths are preserved.

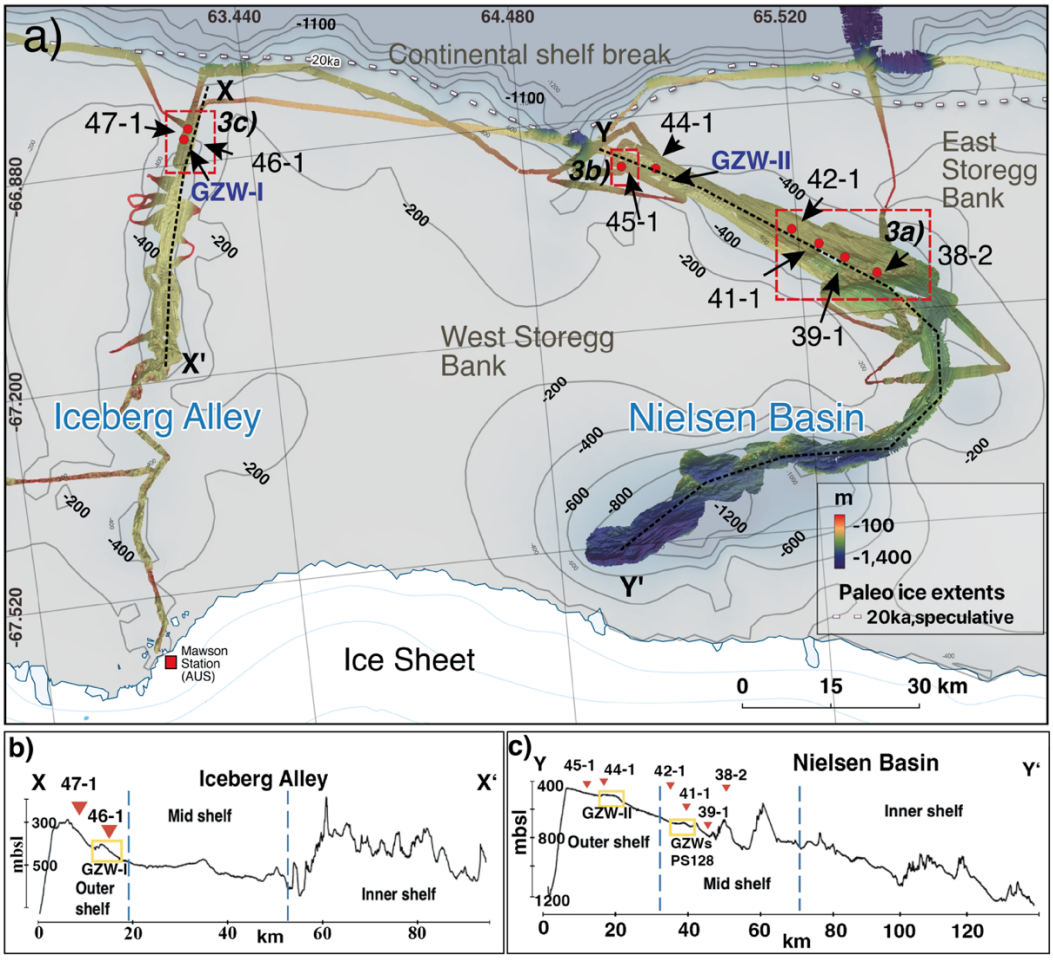

Figure 2: Bathymetric overview of the Mac. Robertson continental shelf; colored depth profile from **MBES for NB and IA (PS128/NBP0101). The bottom row shows vertical cross-sections through the IA (left) and NB (right) basin topography. Red dots indicate core locations (abbreviated for readability), and insets of dashed squares (a-c, italic) are shown in Fig. 3. GZWs in the vertical cross-sections are marked by yellow squares. GZW-I and GZW-II refer to presumed LGM GZW locations suggested by Mackintosh et al. (2011). Basemap modified from IBCSO v2 (Dorschel et al., 2022).**

The Iceberg Alley trough is characterized by elongated, streamlined, (sub)parallel features on its mid shelf and changes towards more randomly oriented curvilinear features on the outer shelf (cf., Leventer et al., 2006; Fig. 3c), including a wedge-like feature previously interpreted as a LGM GZW (Mackintosh et al., 2011; Fig. 3c; i.e., GZW-I). The outer shelf assemblages resemble those identified on the outer Nielsen Basin, including GZW-I (Fig.2; panel a and cross-section panel b; cf. Mackintosh et al. 2011) and NNE-oriented curvilinear and linear features (Fig. 3). It has a height of ~8 m and an along-flow length of 2 km and is superimposed on elongated, streamlined, parallel features (Fig. 3; c). The water depths, crest height, and location on the outer shelf of GZW-I are comparable to GZW-II.

4.2 Interpretation of seafloor geomorphology and sub-seafloor stratigraphy

Based on numerous previous Antarctic shelf studies (e.g., Klages et al., 2014, 2015; Livingstone et al., 2016a; Halberstadt et al., 2016), we interpret the elongated, streamlined, and parallel bedform assemblages identified on the Nielsen Basin mid-shelf as mega-scale glacial lineations (MSGL). These features usually form under wet-based, fast-flowing ice streams on soft, deformable substrates such as glacial tills as a result of till deformation and basal sliding, often underlain by a consolidated, stiff till (e.g., Ó Cofaigh et al., 2007; Reinardy et al., 2011). Differently oriented sets of N-NNW-oriented MSGLs within the curved trough (Fig. 3; a), disrupted by rugged bedrock topography, may imply their multi-temporal formation (e.g., Graham et al. 2009). They show an increase in elongation on the lee side of the bathymetric sill (Fig. 3a). Usually, this is associated with flow acceleration at substrate boundaries and deforming bed conditions (Ó Cofaigh et al., 2007; Graham et al., 2009, Livingstone et al., 2016b; Jamieson et al., 2016). In the absence of sufficiently penetrating sub-bottom profiles, we generalize the teardrop-shaped features on top of the Nielsen Basin bedrock sill to "drumlinoid features" (Fig. 3a), usually associated with ice-flow velocity changes (e.g., Graham et al., 2009). Varying sizes and shapes of MSGLs and drumlinoids likely result from a complex interplay between differences in local substrates, changing ice flow conditions, or small-scale variations in basal conditions (Graham et al., 2009; Greenwood et al., 2021).

The wedge-like features on the Nielsen Basin's mid to outer shelf transition are identified as grounding-zone wedges (GZWs; cf. Fig.2a; Fig.3c and profile X-X'), closely resembling numerous features previously reported from Antarctic continental shelves (e.g., Jakobsson et al., 2012; Klages et al., 2014, 2015, 2017; Batchelor and Dowdeswell, 2015). GZW dimensions are controlled by sediment delivery, duration of stillstand, cavity shape, and the width of the streaming ice margin (e.g., Dowdeswell and Fugelli, 2012; Simkins et al., 2018). In our study area, they co-occur with linear to curvilinear iceberg scours formed by the seafloor-scouring keels of grounded icebergs (Fig. 3b).

In Iceberg Alley, the streamlined, subparallel features from the inner to mid shelf were equally classified as "drumlinoid features". They likely formed similarly to the ones in Nielsen Basin, i.e., from ice flow velocity changes due to varying bedrock composition underneath the streaming ice. On the outer shelf, we identified the clustered parallel ridges as MSGL (Fig. 3c) and the deeper ridges with low parallelism as iceberg scours. Some of the scours are cross-cutting, indicating the presence of large, multidirectional icebergs that were calving close to the ice sheet margin at different timescales. GZW-I on the outer shelf is superimposed on the MSGLs and, therefore, suggests an earlier formation of these MSGLs (Fig. 3c; dotted blue lines).

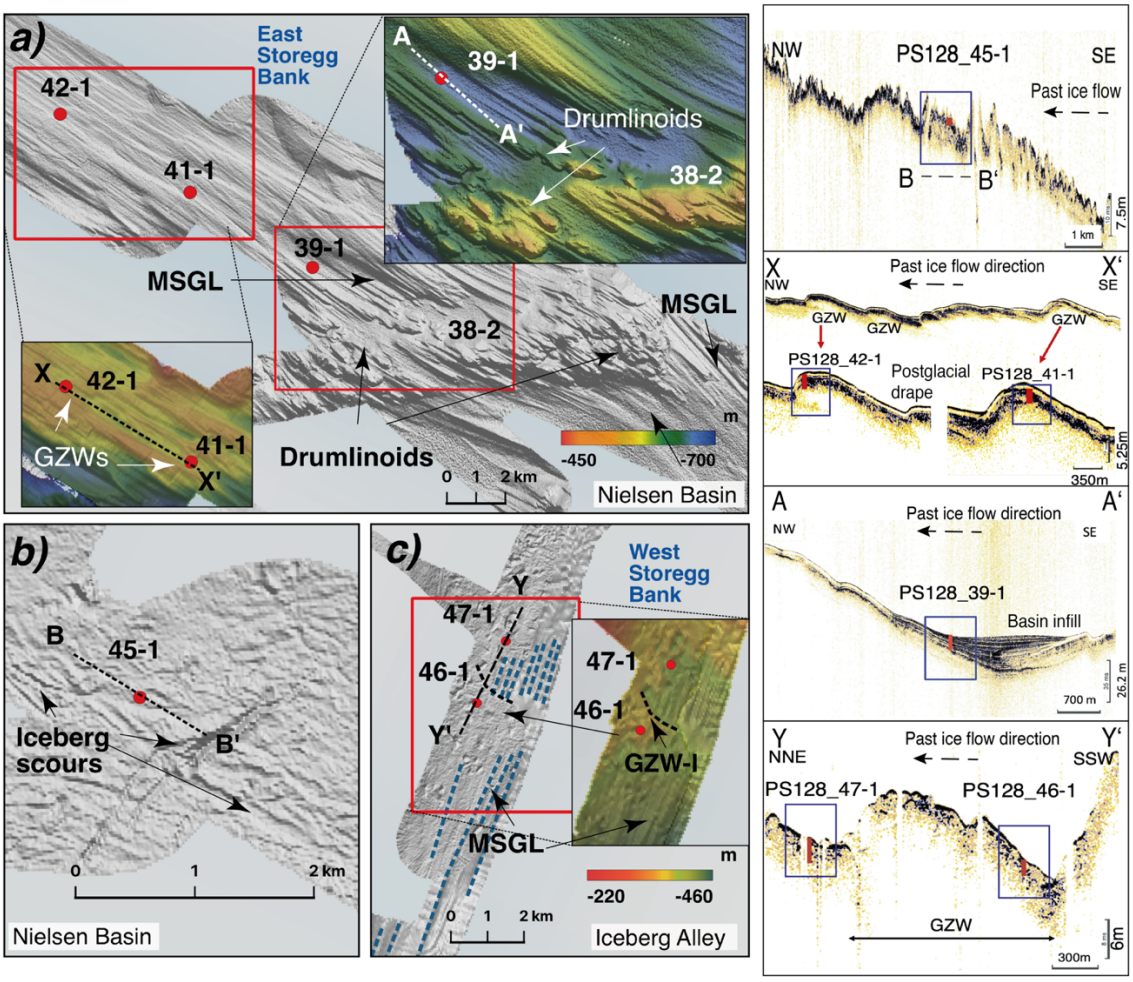

Figure 3: Bathymetric map insets from Fig. 2 (25 x 25 m) with identified submarine glacial landforms of the middle shelf (a: Nielsen Basin) and outer shelf (b: Nielsen Basin, c: Iceberg Alley). Red dots indicate coring locations from Fig. 2 (abbreviated for readability). The PARASOUND profiles are across outer shelf Nielsen Basin (B-B'), mid-shelf GZWs Nielsen Basin (X-X'), the sediment basin seaward the bedrock sill (A-A'), and across outer shelf Iceberg Alley (Y-Y'), with coring locations indicated. The sub-bottom profiles reveal the internal structures of the GZWs (X-X'; Y-Y'), the stratified basin infill (A-A'), and the dotted arrow shows the paleo ice flow direction.

4.3 Facies analyses and chronology of sediment cores

For this study, eight gravity cores were analyzed from the central mid-outer Nielsen Basin and outer Iceberg Alley (Fig. 2) to explore past grounding line extent and subsequent retreat dynamics since the LGM (Fig. 4 & 5; Tables 2 and 3).

The outer shelf gravity cores PS128_45-1 and 44-1 were retrieved near the continental shelf break of Nielsen Basin, and just seaward of GZW-II (cf. Mackintosh et al., 2011; Fig. 2). Mid-shelf cores PS128_42-1 and 41-1 were recovered from the top sets of two GZWs, PS128_39-1 from a sedimentary basin, and PS128_38-2 from a bedrock sill. Gravity cores PS128_46-1

and PS128_47-1 were recovered from outer Iceberg Alley (Fig. 2), with PS128_46-1 from atop GZW-I (cf. Mackintosh et al., 2011; Fig. 2) and PS128_47-1 located just seaward from GZW-I (Fig. 3; c).

4.3.1 Outer shelf sediment cores

The cores from the outer shelf in both troughs (PS128_44-1, 45-1, and 47-1) contain massive diamictons at the base characterized by high shear strengths (> 10 kPa) and magnetic susceptibilities as well as low water (< 30 %) and TOC (< 0.5 %) contents without the presence of *in-situ* microfossils (Fig. 4 & 5; Supplementary Fig. S1). The basal unit in PS128_46-1 reveals a diamicton-like structure in the CT scans (240-262 cmbsf) with angular clasts of different sizes and orientations contained in a fine matrix. Here, magnetic susceptibility values are highest at the base (250 cmbsf) and decrease up-core. From the base toward the surface, the shear strength in PS128_44-1,45-1, and 47-1 drops below 10 kPa, while the water content increases, magnetic susceptibility values vary strongly, and *in-situ* microfossils become more abundant. The unit above the massive diamicton in PS128_45-1 (100-58 cmbsf) is classified as a gravelly sandy mud and shows some degree of stratification. Here, the shear strength drops to zero with a pronounced peak in magnetic susceptibility at 75 cmbsf (Fig. 4). PS128_44-1 revealed a fining-upwards sequence from 220-0 cmbsf from a diamicton to a sandy mud, followed by a coarsening-upwards trend back to a stratified diamicton (Supplementary Fig. S1).

Both Iceberg Alley outer shelf cores, PS128_46-1 and 47-1, show more prominently stratified layers of distinct diatomaceous reddish-brown laminated mud above the boundary from the base (~221-230 cmbsf and 227-254 cmbsf, cf. close-up (red) Fig. 5), which were not found in any of the PS128 Nielsen Basin cores. These stratified to laminated layers are low in sand and gravel content with abundant calcareous and siliceous microfossils (e.g., *Fursenkoina fusiformis, Trifarina* sp., *Cassidulinoides* sp., *Corethron* spp., and *Chaetoceros* spp.). Up-core, the lithology is characterized by bioturbation and an increase in organic matter and water content. In particular, PS128_46-1 and PS128_47-1 are characterized by intense bioturbation, are primarily stratified, and are abundant in calcareous microfossils such as foraminifera, ostracods, bivalves, and bryozoans ("seasonal-open marine facies", Fig. 5).

4.3.2 Mid-shelf sediment cores

Proxies from the basal unit of the mid-shelf cores PS128_42-1 and PS128_38-2 are similar to those of the outer shelf, being characterized by massive diamictons with high shear strengths and magnetic susceptibilities, low water and TOC contents, and no *in-situ* microfossils. In contrast, the basal units of PS128_41-1(from 230 cmbsf) and PS128_39-1 (from 750 cmbsf) are classified as diamictons with low to medium shear strengths of < 5 kPa (Supplementary Fig. S1).

Shear strength decreases further at the up-core boundary above the diamicton, in all mid-shelf cores, while the abundance of *in situ* microfossils increases. Magnetic susceptibility and C:N ratios show pronounced fluctuations, with maxima occurring in the muddy sand layers of cores PS128_41-1 (at 170 cmbsf) and PS128_39-1 (at 400 and 330 cmbsf). Biological activity increases, and stratification is weak or absent (Supplementary Fig. S1). In core PS128_39-1, the sandy mud unit shows an increase in clast content, including several particularly large clasts around 400 cmbsf. From 360 to 330 cmbsf, the lithology

changes with nearly 100 % medium-sized sand, coinciding with the shear strength maxima and the TOC minima, following the magnetic susceptibility peak (Fig. 4).

In the surface unit of all mid-shelf cores, microfossils were abundant, including diatoms, radiolaria, and arenaceous foraminifera (e.g., *Miliammina arenacea*), with calcareous foraminifera present in some cores (e.g., *N. pachyderma, Cassidulinoides* sp.). In cores PS128_39-1 and PS128_41-1, the surface unit is characterized by very low shear strength (0 kPa to < 5 kPa), high water (> 50 %), higher TOC contents, and a distinct lithological transition to stratified diatomaceous oozes from 300 cmbsf and 170 cmbsf up-core, respectively (cf. Fig. 4 & 5; Supplementary Fig. S1).

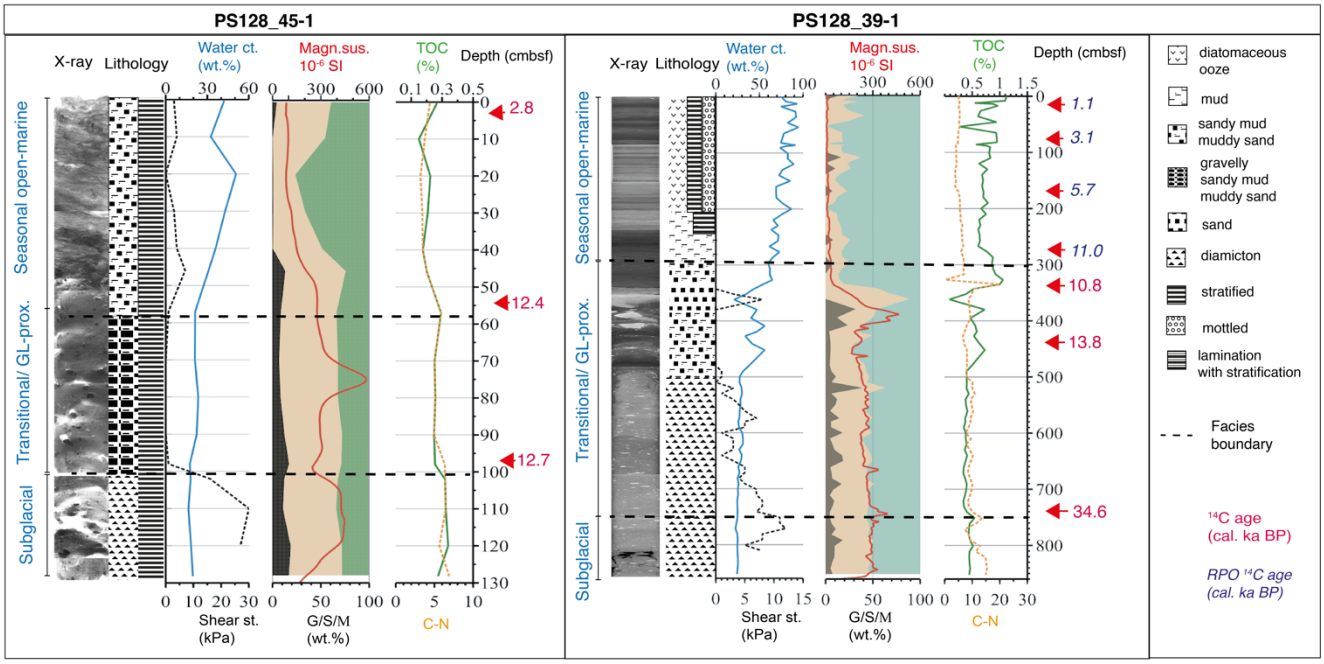

Figure 4: Core parameters of Nielsen Basin mid-shelf core PS128-39-1 and outer shelf core PS128_45-1 (X-Ray, Lithology, Water content wt. %, Shear strength kPa (dotted line), Grain size distribution wt. %; Gravel (G), Sand (S), Mud (M), magnetic susceptibility SI^{-6}, TOC %, C:N (dotted line). Red numbers indicate calibrated foraminifera-derived AMS ^{14}C ages. The dashed lines mark the facies boundaries (Lithological units are named after identified depositional environments).

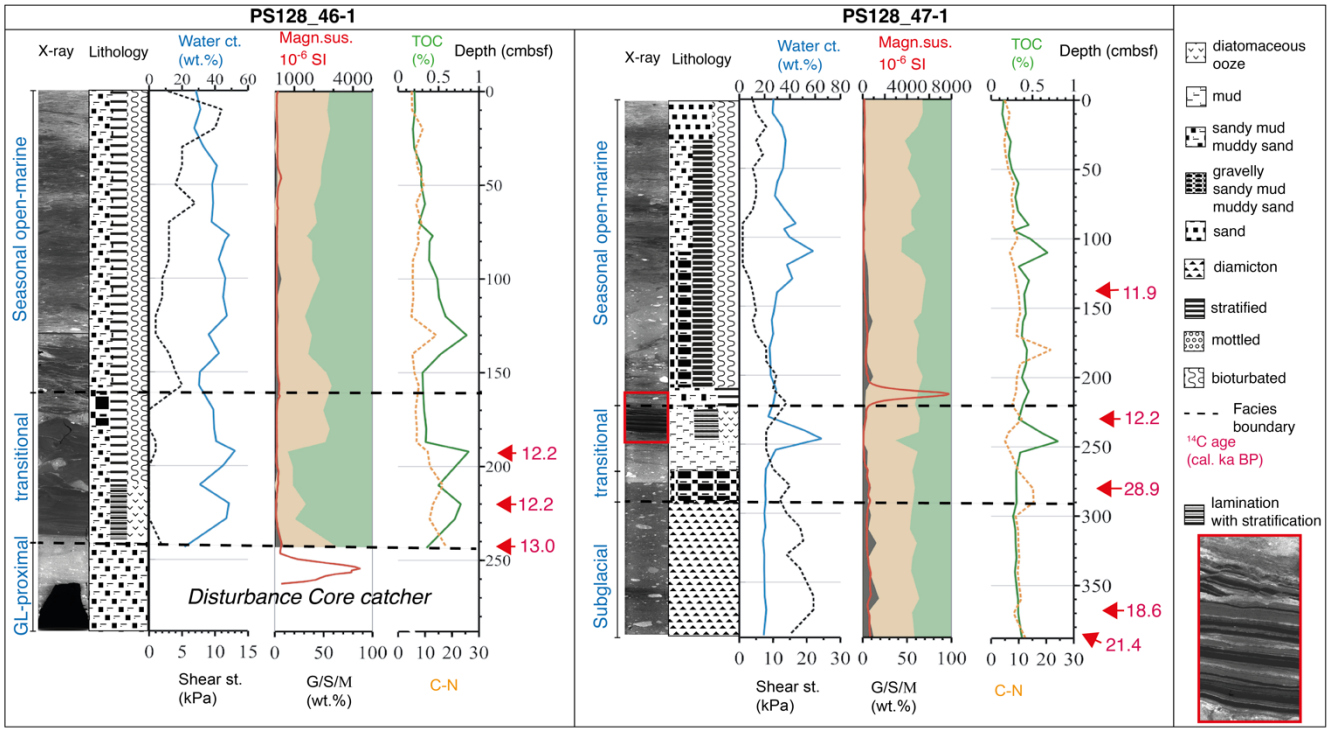

Figure 5: Core parameters of Iceberg Alley shelf cores PS128-46-1 and 47-2 (X-Ray, Lithology, Water content wt. %, Shear strength kPa (dotted line), Grain size distribution wt. %; Gravel (G), Sand (S), Mud (M), magnetic susceptibility SI^{-6}, TOC %, C:N). Red numbers indicate calibrated foraminifera-derived AMS ^{14}C ages. The dashed lines mark the facies boundaries (Lithological units are named after identified depositional environments). The red square marks the close-up, at the bottom of the legend, on the laminations in the transitional facies, which have been previously identified in other Iceberg Alley cores (cf. Leventer et al., 2006; Alley et al., 2018).

4.4 Interpretation of sedimentary depositional environments

The geological record of grounding line retreat in gravity cores from the Antarctic continental shelf is usually evident from three to four sedimentary facies reflecting the changing conditions at a particular site from subglacial over grounding line-proximal and sub-ice shelf to seasonal open-marine deposits (e.g., Hillenbrand et al., 2014; Klages et al., 2013). Ideally, such facies successions can be put into chronological context by dating *in-situ* calcareous microfossils or, if the sedimentary environment allows (Hillenbrand et al., 2010), bulk organic carbon. We assigned depositional settings for the lithological units based on our multi-proxy approach, summarized in Table 2.

4.4.1 Depositional environments of outer shelf sediment cores

Based on the characteristics of the lower lithological unit from the outer shelf cores PS128_44-1, 45-1, and 47-1, we interpret these as subglacial deposited sediments (cf. sect. 4.3; Table 2; e.g., Hillenbrand et al., 2014; Klages et al., 2013). The contained clasts in this unit are mostly metamorphic, hence indicating a subglacial terrigenous supply from the hinterland (e.g., Mackintosh et al., 2007). In core PS128_46-1, a glaciomarine GL-proximal deposition is present at the base of the core.

The increase in water content with decreasing sediment compaction and higher biological activity above the boundary to the basal unit (subglacial till or GL-proximal) in cores PS128_44-1, 45-1, 46-1, and 47-1 indicates a glaciomarine environment (transitional) proximal to the GL (Fig. 4 & 5, cf. Smith et al., 2019). The metamorphic clasts found in these units may result from sub-ice shelf rain-out and/or iceberg calving, and are therefore interpreted as ice-rafted debris (IRD). In PS128_44-1, the transitional facies is characterized by signatures indicative of an ice-shelf break-up, e.g., a massive to stratified sandy, muddy diamicton and an increase in organic matter with the occurrence of some diatoms and foraminifera (cf., Smith et al., 2019; Supplementary Fig. S1). The microfossils found in this zone in cores PS128_46-1 and 47-1 indicate seasonal phytoplankton blooms (*Corethron* spp. and *Chaetoceros* spp. resting spores) likely due to iron-rich meltwater input from iceberg calving, as suggested in previous works from Sedwick et al. (2001), Leventer et al. (2006), and Alley et al. (2018). Additionally, Majewski et al. (2020) assigned the foraminifera *Fursenkoina fusiformis, Trifarina* sp., and *Cassidulinoides* sp., which we found in our transitional facies, as indicative of a meltwater plume or proximal glaciomarine environment (cf. Fig. 5; red close-up view). We interpret the higher abundance of phytoplankton and siliceous foraminifera with an increase in TOC and percentage of mud in the surface unit (seasonal open-marine; Fig. 4, Fig. 5 & Supplementary Fig. S1) of the cores PS128_45-1,46-1, and 47-1 as the onset of more seasonal sea-ice conditions.

4.4.2 Depositional environments of mid-shelf sediment cores

The proxies from the basal unit of the mid-shelf Nielsen Basin cores PS128_42-1 and 38-2 are characterized by a highly compacted, unsorted sediment with dispersed clasts and low organic matter (cf. sect. 4.3, Table 2). We assigned these as a subglacial till (Supplementary Fig. S1). The cores PS128_41-1 and 39-1 show similar characteristics but with less uniform shear strength and C:N values. This suggests more GL- proximal conditions (cf. sect. 4.3, Table 2; Fig. 4; Supplementary S1) with a mixed input from terrestrial and marine sources with low biological activity, suggesting permanent ice-shelf cover proximal to the grounding line (cf. Hillenbrand et al., 2010; Smith et al., 2019). Up-core of the basal facies in PS128_41-1 and 39-1, we interpret the proxies as indicative of transitional conditions with basal melt-out and calving of icebergs from the ice shelf. We identified the large clasts found in the transitional zone of core PS128_39-1 as dropstones, either from the calving front or sub-ice shelf rain-out very close to the grounding line from the ice sheet's base. The proxies of the surface unit in these cores indicate an open marine deposition with seasonal peaks in phytoplankton blooms during sea-ice-free periods (Fig. 4). Abundant microfossils (arenaceous foraminifera, e.g., *Miliammina arenacea*) and the absence of IRD suggest that the GL had already retreated toward the inner shelf.

Table 2: Summary table of characteristic lithofacies with assigned depositional settings (ST=shear strength, water ct.=water content wt. %, MS=magnetic susceptibility, TOC=total organic carbon, GL=grounding line, IRD= ice-rafted debris).

Unit	Lithofacies/ Structure	Parameters	Interpreted depositional setting and processes
Subglacial	Diamicton massive	High ST (>10 kPa), medium to low water ct., high uniformly distributed MS, TOC < 0.5, medium C:N, metamorph, crystalline gravels	Massive ice-contact sediment, unsorted and poorly rounded crystalline gravel in a fine matrix. Highly compacted with no in-situ to sparce reworked poorly preserved microfossils: **Subglacial till**
GL-proximal	Diamicton stratified	Low to medium ST (<10 kPa), Water ct. < 40, High MS, TOC < 0.7, Low to medium C:N, metamorph crystalline gravels	Stratified ice-contact sediment, crystalline gravel in a fine matrix, some microfossils, less compacted sediment: **GL proximal/ sub-ice shelf diamicton**
Transitional	Gravelly muddy sand stratified	Medium to high ST (5-15 kPa), Water ct. < 60, High MS, TOC < 0.6, Medium C:N, high clast content, increasing amout of larger sized clasts	High clast content from icebergs (IRD) or rain-out from basal ice shelf, high microfossil content: **Sub-ice shelf close to calving line / seasonal open-marine close to calving line**
Transitional/ seasonal open-marine	Sandy mud stratified	Low ST (<5kPa), Water ct. 25-50, Moderate MS, TOC < 0.7, Medium C:N, Low clast content	Hemipelagic deposition with high microfossil content sometimes alternating settling of diatom-bearing sediments: **Sub-sea ice to seasonal open-marine**
Transitional/ seasonal open-marine	Muddy sand stratified and non-stratified	Low to medium ST (<10 kPa), in parts high ST (>15 kPa), Low to medium water ct., Low MS, TOC< 1.0, high C:N, low clast content	Hemipelagic deposition sometimes stratified or bioturbated: Fine-grained hemipelagic sediments, high microfossils (planktic foraminifera), clasts from sub-ice shelf melt-out or calving: **Sub-sea ice to seasonal open-marine**
Seasonal open-marine	Mud stratified	Low ST (< 5 kPa), Water ct. > 50, Low MS, TOC > 0.6, Low C:N No clasts	Fine-grained hemipelagic sediments, high microfossils (planktic foraminifera) and organic matter content, few IRD probably melt-out from sea-ice: **Seasonal open-marine**
Seasonal open-marine	Mud Diatom-bearing mottled	Low to medium ST (<10 kPa), Water ct. > 50, Low MS, TOC > 0.5, Low C:N No clasts	Alternating settling of glaciomarine hemipelagic and meltwater plume material, high microfossil content: **Sub-sea ice to Seasonal open-marine, meltwater induced**
Seasonal open-marine	Diatomaceous ooze mottled stratified	Low ST (0 kPa), Water ct. > 60, Low MS, TOC > 0.7, Low C:N No clasts	Alternating settling of pelagic material indicating annual phytoplankton blooming events, high abundance in diatoms: **Seasonal open-marine**

Our ^{14}C ages support our facies interpretation, and we suggest a retreat just before ~12.7 cal. ka BP from the Nielsen Basin outer shelf right above the transition from the subglacial till to the transitional sediments, i.e., sediments that deposited right after the GL retreated from the location PS128_45-1 (98 cmbsf). The transition from subglacial till to transitional sediments in core PS128_47-1 reveals ages around ~12.2 cal. ka BP (230 cmbsf), suggesting a similar retreat age in Iceberg Alley. Core PS128_39-1 indicates varying GL sediment discharge in the transitional depositional environment (750-300 cmbsf) around ~13.8 cal. ka BP, while the seasonal open-marine facies above 300 cmbsf is dated with ~10.8 cal. ka BP, marking the onset of Holocene conditions (see Table 3). Above this boundary, sedimentation changes from lower to higher rates, which is characteristic of deglacial sediments. The RPO ages from the diatomaceous oozes in the seasonal open-marine facies (0-300 cmbsf) range from 1.1 cal. ka BP to 11.0 cal. ka BP (Table 3). These ages underline our assumption of a GL retreat somewhere between 11.0 and 10.8 cal. ka BP, and the onset of the diatomaceous oozes indicates seasonal open-marine conditions around the start of the Holocene.

The AMS ^{14}C dates of the sediment cores are listed as conventional ages and calibrated ages in Table 3, including the error and median values.

Table 3: Conventional and calibrated ^{14}C ages of PS128 and recalibrated JPC40, JPC43B and PS69/849-2 cores with Calib 8.2 (Stuiver and Reimer, 1993). Reservoir correction for glacial samples 1,300 (+-100) and Marine20 calibration curve (Heaton et al., 2020). Ages in bold are the minimum age constraints (*in situ* foraminifera) and bold italics are possible maximum ages (reworked foraminifera found in subglacial till) used for paleo-grounding line reconstruction. NB = Nielsen Basin, IA = Iceberg Alley, BB=Burton Basin, AIO = Acid insoluble organic matter, RPO=Ramped-pyrolysis-Oxidation

Core Nr./ position	Depth (cmbsf)	Location Shelf	Dated material	Conventional radiocarbon ages (^{14}C ka BP) +- error	Calibrated radiocarbon ages Age range (cal. ka BP) 2 sigma rounded	Median (cal. ka BP) rounded
PS128_39-1	**352**	Mid Shelf NB	Benthic foraminifera	**10,719 +-238**	**10,200-11,500**	**10,800**
PS128_39-1	452		Benthic foraminifera	13,150 +-112	13,500-14,100	13,800
PS128_39-1	741		Benthic foraminifera	31,731 +-755	33,000-36,200	***34,600***
RPO ages PS128_39-1						
286°C	4.5		Bulk sediment	1,708+-75	920-1,300	1,100
294°C	79.5		Bulk sediment	3,381+-78	2,800-3,300	3,100
293°C	178.5		Bulk sediment	5,464+-88	5,400-5,900	5,700
287°C	284.5		Bulk sediment	10,010+-109	10,600-11,200	**11,000**
294°C	338.5		Bulk sediment	11,571+-173	11,500-12,600	12,100
283°C	348.5		Bulk sediment	11,990+-177	12,100-13,000	12,600
PS128_45-1	1	Outer Shelf NB	Planktic foraminifera	3,153 +- 60	2,600 – 3,000	2,800
PS128_45-1	57		Benthic foraminifera	11,802 +-30	12,200 – 12,600	12,400
PS128_45-1	98		Benthic foraminifera	**12,169 +-31**	**12,600 - 12,900**	**12,700**
PS128_47-1	140	Outer Shelf IA	Benthic foraminifera	11,454 +-105	11,500-12,300	11,900
PS128_47-1	230		Benthic foraminifera	**11,669 +-105**	**11,900-12,600**	**12,200**

PS128_47-1	268		Benthic foraminifera	39,619 +-920	40,800-43,100	42,000
PS128_47-1	280		Benthic foraminifera	26,270 +-279	28,200-29,600	***28,900***
PS128_47-1	370		Benthic foraminifera	16,896 +- 142	18,200-19,000	18,600
PS128_47-1	388		Benthic foraminifera	19,192 +-169	21,000-21,900	21,400
Recalibrated radiocarbon ages from previous studies on the Mac. Robertson continental shelf						
JPC40-NB	2141	Mid Shelf NB	AIO	13,520	13,900- 14,800	14,300
JPC43B-IA	2310-2315	Mid-outer Shelf IA	AIO	11,770	12,100- 12,600	12,400
PS69/849-2-BB	275	Mid Shelf BB	AIO	12,030 +-90	12,200-12,700	12,500

5 Discussion

5.1 Maximum extent and episodic grounding line retreat since the LGM

Previous studies from around the Antarctic continental shelf suggest a grounded ice sheet at or close to the continental shelf break at the LGM (e.g., Wellner et. al., 2006; Anderson et al., 2014; Hillenbrand et al.,2014; Hodgson et al., 2014; Larter et al., 2014; Mackintosh et al., 2014; Ó Cofaigh et al., 2014; Klages et al., 2014, 2015, 2017), with only a few studies around the East Antarctic margin focusing on grounding line retreat since the Last Glacial Maximum. For the Mac. On the Robertson continental shelf, previous studies revealed characteristic glacial sedimentary deposits in the outer Nielsen Basin, as well as prominent deglacial deposits of alternating laminations of iron-rich sediments and diatomaceous oozes in cores from both inner shelves (Harris and O'Brien 1998; Leventer et al. 2006). Previously, only bulk AIO radiocarbon ages were available, and carbonate ages from foraminifera are a big improvement on those age constraints, because the carbonate retrieved from calcareous microfossils formed *in situ*. Our multi-proxy dataset, including foraminifera-derived ^{14}C age constraints, indicates that grounding lines of fast-flowing ice streams within Nielsen Basin and Iceberg Alley reached the shelf break prior to ~12.7 cal. ka BP (Table 3; Fig. 6a; Fig. 3). The multiple generations of keel scours documented on the outer shelf indicate several calving events of different stages of ice retreat in varying water depths and different constraints on drift directions. The scours are interpreted to be of Holocene age, due to their westward orientation, implicating a drift caused by the current-day configuration of outer shelf currents without lateral constraints from ice bodies (Harris and O'Brien, 1998; Leventer et al., 2006). Our foraminifera-derived ^{14}C age in cores PS128_45-1, 46-1, and 47 from the GL-proximal facies indicates a minimum retreat age of the GL around ~12.2 to 12.7 cal. ka BP from the outer shelf towards the mid-shelf in both basins. This implies that GZW-I and GZW-II (Fig. 2) did not form during the LGM and are post-LGM features. We assume a formation of these GZWs shortly after ~12.7 cal. ka BP. The overprinted MSGLs (Fig. 3c, blue dotted lines) indicate fast-streaming wet-based ice before the formation of GZW-I. Thus, we propose a nearly synchronous initial retreat of the GL from the outer shelf in both glacial troughs (Fig. 6a). A lateral narrowing of the trough might have slowed down ice retreat due to lateral pinning on the shallower banks on each side of the trough and after the lateral pinning of the ice sheet, conditions favored GZW formation

(Fig. 6b), because lateral and vertical bathymetric pinning points are important factors slowing down ice retreat (Batchelor and Dowdeswell, 2015) and is in accordance with the finding that commonly during the last deglaciation, grounded ice remained on shallow marine areas and adjacent islands, while faster retreat occurred in deeper marine troughs (Dyke et al., 2003). Both troughs significantly deepen into retrograde slopes at the transition from the outer to the mid-shelf. Here, MSGLs are abundant, indicating a fast-flowing ice stream at the time of formation. We inferred an acceleration of GL from the trough topography and the narrow time difference between the ^{14}C ages retrieved from the transitional facies in core PS128_45-1 and PS128_39-1. In Nielsen Basin, we identified several stabilization events on the mid-shelf during GL retreat. The small size and close spacing of the identified GZWs (Fig. 3; Profile X-X') point toward only a short ice sheet stabilization at the transition from the outer shelf to the mid-shelf and the mid-shelf GZWs are likely deposited after ice sheet pinning to outcropping bedrock (Fig. 6c).

Earlier work by Leventer et al. (2006) reveals an AIO age of ~12.4 cal. ka BP for the onset of the deglaciation at the outer-mid-shelf boundary in Iceberg Alley, and Borchers et al. (2016) propose a similar AIO deglaciation age (~12.5 cal. ka BP) for the mid-shelf region in Burton Basin. These ages are almost identical to ours (~12.7 cal. ka BP), and this strengthens the assumption of a nearly synchronous grounding line retreat across the Mac. Robertson continental shelf. Yet, comparisons between AIO and foraminifera-derived ^{14}C ages need to be treated tentatively, because AIO dates are often affected by contamination from reworked fossil carbonate, resulting in older AMS ages with a drastic down-core increase in ^{14}C ages (Andrews et al., 1999). We attribute the older ^{14}C ages from core JPC40 to entrained carbon in the bulk samples, leading to a modified deglaciation age. However, we cannot completely rule out the possibility that the outer shelf deglaciation started earlier, between 13 and 14 ka BP. Our additional RPO ages in core PS128_39-1 (blue ages in Fig. 4) help to better constrain the onset of deglaciation for the Nielsen Basin's mid-shelf. Here, the reworking of our foraminifera-derived carbonate material proximal to the retreating GL complicates the constraint on the exact timing. The material in the transitional/GL-proximal facies in PS128_39-1 is composed of glacially-transported sediments with unsorted grain sizes, transitioning into a slightly stratified sediment with big dropstones and a prominent sand layer. From the depositional environment and the regional topography, we inferred a varying GL during this time, depositing subglacial sediments downhill in front of the sill. Bioturbation marks at the depths of ~350 to 330 cmbsf can be explained by increased biological activity after the GL retreated farther from the sill. The RPO ages above 330 cmbsf of 11.0 cal. ka BP indicates the onset of the Holocene. This strengthens the foraminifera-derived ages of 10.8 cal. ka BP retrieved at this interval. The ^{14}C ages retrieved from some sparse specimens (*Globocassidulina sp*.) in the GL-proximal of PS128_47-1 indicate an age of ~28.9 cal. ka BP (Iceberg Alley) and the subglacial till in PS128_39-1 of ~34.6 cal. ka BP (Nielsen Basin). These specimens are likely reworked but still radiocarbon active. We cautiously propose this as a maximum glaciation age from older entrained microfossils in the subglacial till.

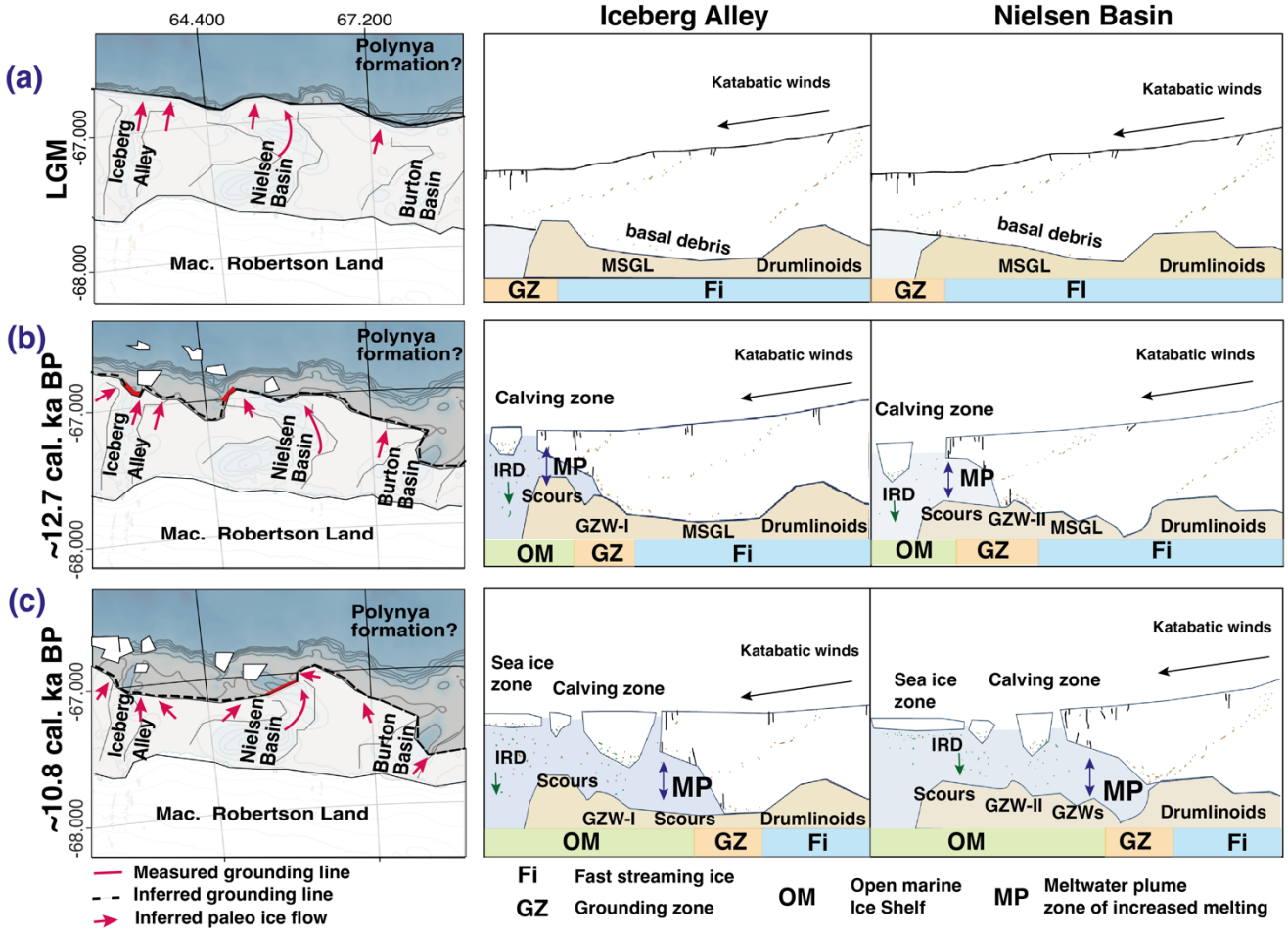

Figure 6: Conceptual model of grounding line extent and retreat on the Mac. Robertson continental shelf for the LGM (a) to just before ~12.7 cal. ka BP, (b) ~12.7 to just before ~10.8 cal. ka BP and (c) shortly after ~10.8 cal. ka BP. The ice sheet's grounding line extent is illustrated on the continental shelf for the three main basins (left) with measured paleo-grounding line (red) and inferred grounding line on adjacent inter-ice stream ridges (dashed black line). Red arrows indicate reconstructed ice flow directions inferred from basin topography and bedform orientation. The vertical cross-section through Iceberg Alley (IA) and Nielsen Basin (NB) is illustrated (right) based on facies analysis of sediment cores, ^{14}C ages, and glacial bedforms (schematic representation; not to scale).

5.2 Wider context of Mac. Robertson continental shelf deglaciation and relevance for AABW formation

Reliable deglaciation ages are sparse for East Antarctic continental shelves, and because GL retreat around Antarctica results from several driving forces, such as oceanic conditions, bathymetry, prior ice extent, and ice sheet thickness, as well as bottom substrate composition, the overall ice sheet retreat varies widely between different regions. In comparison to the deglaciation history of Prydz Bay, where the continental shelf break of the Prydz Channel in front of the Amery Ice Shelf was already ice-free at the LGM (Domack et al.,1998; Hemer and Harris, 2003; Guitard et al., 2016), the Mac. Robertson continental shelf

appears to have remained glaciated for a substantially longer period. Regional differences in bathymetric configuration likely contributed to these contrasting retreat histories around Antarctica. For example, GL retreat is facilitated and accelerated on retrograde sloping beds and topography below sea level. Such retrograde slopes are less pronounced across much of the East Antarctic continental shelf, except within cross-shelf glacial troughs (Morlighem et al., 2020). In addition to bathymetry, the intensity of mCDW intrusions onto the continental shelf controls the timing and intensity of the retreat. This is influenced by the stratification and composition of the water column, as well as by prevailing currents at the continental shelf break, and facilitated by oceanic gateways (Nicola et al., 2025). Isopycnals, stratified density layers of the ocean, at the shelf break influence which water masses can access or ventilate the shelf. Thompson et al. (2018) classified the East Antarctic area around the Mac. Robertson continental shelf as a "dense shelf" regime. This oceanic regime is characterized by persistent strong easterly winds and a westward-flowing ASC. Here, strong fronts separate cold and fresh shelf water from warm and salty CDW offshore, leading to a weak cross-slope exchange of water masses. In this regime, it is much harder for mCDW to intrude onto the shelf compared to a "warm shelf" regime, which prevails around most of, e.g., West Antarctic continental shelves (Thompson et al., 2018). This may likewise have limited the intrusion of mCDW onto the shelf in East Antarctica in the recent past. Our deglaciation age of the Mac. Robertson continental shelf of ~12.7 cal. ka BP coincides with the end of the Antarctic Cold Reversal (ACR), a temporary atmospheric and oceanic cooling in the Southwest Pacific due to deglacial changes in the Atlantic Meridional overturning circulation, while a warming occurred in the Northern Hemisphere (Eaves et al. 2024), and it lasted from ~ 14.5 to ~13.0 ka BP (Pedro et al., 2016). Our deglaciation ages reveal an onset at the end or shortly after this short-term cooling interval. The initial retreat age of ~12.7 cal. ka BP is too late (after 14.2 ka BP) to be assigned to the rising sea level from Meltwater Pulse 1a (MWP-1a). Yet, the sea level rise during Meltwater Pulse 1b (MWP-1b), triggered by elevated meltwater discharge and the disintegration of large parts of the ice sheet between 11.5 and 11.2 ka BP (Peltier et al., 2006), falls into the same time interval as our deglaciation ages. This additional sea level rise may have lifted the depth interval in which the CDW resides. The complex topography of the Mac. Robertson continental shelf, with Nielsen Basin and Iceberg Alley as deeper cross-shelf troughs, might have provided geostrophic pathways for mCDW to enter the continental shelf (cf. Fig. 6b). Additionally, southward migration of westerly winds and stronger coastal easterly winds might have enhanced upwelling (Fripiat et al., 2026) and the westward-flowing coastal current (Kusahara et al., 2017). All of the above may have delayed CDW intrusion onto the continental shelf, and in combination with the regional topography, lead to a more resilient ice sheet, delaying GL retreat on the Mac. Robertson continental shelf. Based on our multi-proxy analyses, we therefore propose a fully glaciated continental shelf during the LGM, which would imply absent DSW production on the shelf. This implies a different formation area of AABW, e.g., polynyas beyond the continental shelf break, farther offshore.

To get a better understanding of the forcing mechanisms driving ice sheet retreat, future studies might investigate grounding line retreat and advance of outer shelf deglaciation from adjacent areas along the East Antarctic Indian and Atlantic margin to connect grounding line retreat patterns. Volume estimations of past ice sheets on the East Antarctic shelves by combining terrestrial cosmogenic exposure dates with marine radiocarbon measurements might complete the overall picture of past ice sheet dynamics.

6 Conclusion

Our study is the first to combine a multi-proxy approach of geochemical, geophysical, and sedimentological data for a transect through the Nielsen Basin and Iceberg Alley. Thus, it provides new insights into ice sheet grounding line dynamics on the Mac. Robertson continental shelf, including the timing determined from AMS ^{14}C ages, exclusively from foraminiferal carbonate. This allows the creation of reliable spatiotemporal benchmarks for ice sheet simulations for the Nielsen Basin. Further, it allows a reliable determination of the grounding line retreat from the outer shelf in Iceberg Alley. We conclude the presence of a wet-based fast-flowing ice stream and episodic ice sheet retreat with several stabilization phases for both troughs from the LGM to today. Furthermore, the ^{14}C ages of core PS128_45-1 and PS128_47-1 with a deglaciation age of ~12.2 - 12.7 cal. ka BP contradicts a presumed LGM age of both GZW-I and GZW-II on the Mac. Robertson continental shelf, leading to the assumption of an ice sheet grounded at the Mac. Robertson continental shelf break during the LGM. This likely would have resulted in absent DSW formation at the Cape Darnley Polynya and, thus, AABW formation, leading to another formation area off the continental shelf.

Data availability The metadata of sediment cores (https://doi.pangaea.de/10.1594/PANGAEA.982379) and multibeam bathymetric data (https://doi.org/10.1594/PANGAEA.954693) presented are available at the PANGAEA data repository.

Supplements

Figure S1**:** Core parameters of Nielsen Basin cores PS128_38-2, 41-1,42-1 and 44-1 (X-ray, Lithology, Shear strength, Water ct., TOC, C:N, Grain size)

Table S1: Full list of all measured conventional and calibrated ^{14}C ages and full description of Ramped Pyrolysis Oxidation (RPO).

Author contribution J.G. participated in conceptualizing, data sampling, data analysis and interpretation, as well as visualization and writing of the manuscript. J.M. was involved in expedition planning, core recovery and data analysis. R.T. was involved in expedition planning and core recovery. G.M. was involved in core recovery and the radiocarbon analysis. L.L-J. was involved in core recovery and data analysis. E.W. was responsible for the PARASOUND data collection and visualization. L.S and N.W. participated partly in data analysis. L.K. participated in the radiocarbon analysis. A.M. was involved in cruise planning and data discussion. J.P.K. was responsible for conceptualization, cruise planning, core recovery, supervision, data collection, analysis, and interpretation. All authors took part in the discussion of the manuscript. All authors read the manuscript, commented on the submitted version, and agreed to its submission.

Competing interests The authors declare that they have no conflict of interest.

Acknowledgements We thank the captain and crew of RV *Polarstern* Expedition PS128 "EASI-1" (Grant Number PS128_00) as well as V.Schumacher, P.Daub, H.Roeben, Y.Schulze-Tenberge and M. Seebeck for their diligent help on board and in the lab. We also thank C.Gebhardt and T.Bozkuyu for the processing of the MSCL data and F. Nitsche for providing the NBP0101 bathymetric grids.

Financial support J.G. has been supported by the International Science Program for Integrative Research in Earth Systems (INSPIRES IV) at the Alfred Wegener Institute, Helmholtz Centre for Polar and Marine Research. J.M., R.T., L.L.-J., G.M., E.W., J.P.K. were funded by the Helmholtz Association's Research Program "Changing Earth–Sustaining our Future". L.K. received support from the International Science Program for Integrative Research in Earth Systems (INSPIRES III) at the Alfred Wegener Institute, Helmholtz Centre for Polar and Marine Research. A.M. was supported by the Australian Research Council (ARC) SRIEAS grant SR200100005, Securing Antarctica's Environmental Future.

References

Alley, K., Patacca, K., Pike, J., Dunbar, R., and Leventer, A.: Iceberg Alley, East Antarctic Margin: Continuously laminated diatomaceous sediments from the late Holocene, Mar. Micropaleontol. , 140, 56–68, https://doi.org/10.1016/j.marmicro.2017.12.002, 2018.

Anderson J.B, Shipp S.S, Lowe A.L, Wellner J.S, Mosola A.B: The Antarctic ice sheet during the last glacial maximum and its subsequent retreat history: a review. Quatern Sci Rev 21:49–70. https://doi.org/10.1016/S0277-3791(01)00083-X, 2002.

Anderson, J. B., Conway, H., Bart, P. J., Witus, A. E., Greenwood, S. L., McKay, R. M., Hall, B. L., Ackert, R. P., Licht, K., Jakobsson, M., and Stone, J. O.: Ross Sea paleo-ice sheet drainage and deglacial history during and since the LGM, QSR, 100, 31–54, https://doi.org/10.1016/j.quascirev.2013.08.020, 2014.

Andrews, J. T., Domack, E. W., Cunningham, W. L., Leventer, A., Licht, K. J., Jull, A. J. T., DeMaster, D. J., and Jennings, A. E.: Problems and Possible Solutions Concerning Radiocarbon Dating of Surface Marine Sediments, Ross Sea, Antarctica, Quaternary Res., 52, 206–216, https://doi.org/10.1006/qres.1999.2047, 1999.

Arndt, J. E., Hillenbrand, C.-D., Grobe, H., Kuhn, G., and Wacker, L.: Evidence for a dynamic grounding line in outer Filchner Trough, Antarctica, until the early Holocene, Geol., 45, 1035–1038, https://doi.org/10.1130/G39398.1, 2017.

AWI. Alfred-Wegener-Institut Helmholtz-Zentrum für Polar- und Meeresforschung (AWI).: Polar Research and Supply Vessel Polarstern Operated by the Alfred-Wegener-Institute. Journal of large-scale research facilities, 3, A119. http://dx.doi.org/10.17815/jlsrf-3-163. 2017.

Batchelor, C. L. and Dowdeswell, J. A.: Ice-sheet grounding-zone wedges (GZWs) on high-latitude continental margins, Marine Geol., 363, 65–92, https://doi.org/10.1016/j.margeo.2015.02.001, 2015.

Berkman, P. A. and Forman, S. L.: Pre-bomb radiocarbon and the reservoir correction for calcareous marine species in the Southern Ocean, Geophysical Research Letters, 23, 363–366, https://doi.org/10.1029/96GL00151, 1996.

Borchers, A., Dietze, E., Kuhn, G., Esper, O., Voigt, I., Hartmann, K., and Diekmann, B.: Holocene ice dynamics and bottom-water formation associated with Cape Darnley polynya activity recorded in Burton Basin, East Antarctica, Mar Geophys Res, 37, 49–70, https://doi.org/10.1007/s11001-015-9254-z, 2016.

Bradley, A. T. and Hewitt, I. J.: Tipping point in ice-sheet grounding-zone melting due to ocean water intrusion, Nat. Geosci., https://doi.org/10.1038/s41561-024-01465-7, 2024.

Domack, E., O'Brien, P., Harris, P., Taylor, F., Quilty, P. G., Santis, L. D., and Raker, B.: Late Quaternary sediment facies in Prydz Bay, East Antarctica and their relationship to glacial advance onto the continental shelf, Ant. Sci., 10, 236–246, https://doi.org/10.1017/S0954102098000339, 1998.

Dorschel, B., Hehemann, L., Viquerat, S., Warnke, F., Dreutter, S., Schulze Tenberge, Y., Accettella, D., An, L., Barrios, F., Bazhenova, E. A., Black, J., Bohoyo, F., Davey, C., de Santis, L., Escutia Dotti, C., Frémand, A. C., Fretwell, P. T., Gales, J. A., Gao, J., Gasperini, L., Greenbaum, J. S., Henderson Jencks, J., Hogan, K. A., Hong, J. K., Jakobsson, M., Jensen, L., Kool, J., Larin, S., Larter, R. D., Leitchenkov, G. L., Loubrieu, B., Mackay, K., Mayer, L., Millan, R., Morlighem, M., Navidad, F., Nitsche, F.-O., Nogi, Y., Pertuisot, C., Post, A. L., Pritchard, H. D., Purser, A., Rebesco, M., Rignot, E., Roberts, J. L., Rovere, M., Ryzhov, I., Sauli, C., Schmitt, T., Silvano, A., Smith, J. E., Snaith, H., Tate, A. J., Tinto, K., Vandenbossche, P., Weatherall, P., Wintersteller, P., Yang, C., Zhang, T., and Arndt, J. E.: The International Bathymetric Chart of the Southern Ocean Version 2 (IBCSO v2), PANGAEA [data set], https://doi.org/10.1594/PANGAEA.937574, 2022.

Dowdeswell, J. A. and Fugelli, E. M. G.: The seismic architecture and geometry of grounding-zone wedges formed at the marine margins of past ice sheets, Geol Soc Am Bull, 124, 1750–1761, https://doi.org/10.1130/B30628.1, 2012.

Dowdeswell, J. A., Canals, M., Jakobsson, M., Todd, B. J., Dowdeswell, E. K., and Hogan, K. A.: The variety and distribution of submarine glacial landforms and implications for ice-sheet reconstruction, J. Geol. Soc, Memoirs, 46, 519–552, https://doi.org/10.1144/M46.183, 2016.

Dyke, A.S., Moore, A., Robertson, L.: Deglaciation of North America. Geological Survey of Canada. https://doi.org/10.4095/214399. Open File 1574, 2003

Eaves, S. R., Mackintosh, A. N., Pedro, J. B., Bostock, H. C., Ryan, M. T., Norton, K. P., Hayward, B. W., Anderson, B. M., He, F., Jones, R. S., Lorrey, A. M., Newnham, R. M., Tims, S. G., and Vandergoes, M. J.: Coupled atmosphere-ocean response of the southwest Pacific to deglacial changes in Atlantic meridional overturning circulation, Earth Planet. Sci. Lett., 641, 118802, https://doi.org/10.1016/j.epsl.2024.118802, 2024.

Fretwell, P., Pritchard, H. D., Vaughan, D. G., Bamber, J. L., Barrand, N. E., Bell, R., Bianchi, C., Bingham, R. G., Blankenship, D. D., Casassa, G., Catania, G., Callens, D., Conway, H., Cook, A. J., Corr, H. F. J., Damaske, D., Damm, V., Ferraccioli, F., Forsberg, R., Fujita, S., Gim, Y., Gogineni, P., Griggs, J. A., Hindmarsh, R. C. A., Holmlund, P., Holt, J. W., Jacobel, R. W., Jenkins, A., Jokat, W., Jordan, T., King, E. C., Kohler, J., Krabill, W., Riger-Kusk, M., Langley, K. A., Leitchenkov, G., Leuschen, C., Luyendyk, B. P., Matsuoka, K., Mouginot, J., Nitsche, F. O., Nogi, Y., Nost, O. A., Popov, S. V., Rignot, E., Rippin, D. M., Rivera, A., Roberts, J., Ross, N., Siegert, M. J., Smith, A. M., Steinhage, D., Studinger, M., Sun, B., Tinto, B. K., Welch, B. C., Wilson, D., Young, D. A., Xiangbin, C., and Zirizzotti, A.: Bedmap2: improved ice bed, surface and thickness datasets for Antarctica, Cryosphere, 7, 375–393, https://doi.org/10.5194/tc-7-375-2013, 2013.

Fripiat, F., Sigman, D. M., Ai, X. E., Dumoulin, C., Moretti, S., Studer, A. S., Diekmann, B., Esper, O., Frederichs, T., Lamy, F., Liu, L., Pattyn, F., Schmitt, M., Tiedemann, R., Haug, G. H., and Martínez-García, A.: Deglacial stratification of the polar Southern Ocean, Proc. Natl. Acad. Sci. U.S.A., 123, e2502076123, https://doi.org/10.1073/pnas.2502076123, 2026.

Graham, A. G. C., Larter, R. D., Gohl, K., Hillenbrand, C.-D., Smith, J. A., and Kuhn, G.: Bedform signature of a West Antarctic palaeo-ice stream reveals a multi-temporal record of flow and substrate control, QSR, 28, 2774–2793, https://doi.org/10.1016/j.quascirev.2009.07.003, 2009.

Greenwood, S. L., Simkins, L. M., Winsborrow, M. C. M., and Bjarnadóttir, L. R.: Exceptions to bed-controlled ice sheet flow and retreat from glaciated continental margins worldwide, Sci. Adv., 7, eabb6291, https://doi.org/10.1126/sciadv.abb6291, 2021.

Guitard, M. E., Shevenell, A. E., Lavoie, C., and Domack, E. W.: Mega-scale glacial lineations and grounding-zone wedges in Prydz Channel, East Antarctica, J. Geol. Soc , Memoirs, 46, 185–186, https://doi.org/10.1144/M46.110, 2016.

Harris, P. T. and O'Brien, P. E.: Bottom currents, sedimentation and ice-sheet retreat facies successions on the Mac Robertson shelf, East Antarctica, Mar. Geol. 151, 47–72, https://doi.org/10.1016/S0025-3227(98)00047-4, 1998.

Halberstadt, A. R. W., Simkins, L. M., Greenwood, S. L., and Anderson, J. B.: Past ice-sheet behaviour: retreat scenarios and changing controls in the Ross Sea, Antarctica, The Cryosphere, 10, 1003–1020, https://doi.org/10.5194/tc-10-1003-2016, 2016.

Hauck, J., Gerdes, D., Hillenbrand, C.-D., Hoppema, M., Kuhn, G., Nehrke, G., Völker, C., and Wolf-Gladrow, D. A.: Distribution and mineralogy of carbonate sediments on Antarctic shelves, J. Mar. Syst, 90, 77–87, https://doi.org/10.1016/j.jmarsys.2011.09.005, 2012.

Heaton, T. J., Köhler, P., Butzin, M., Bard, E., Reimer, R. W., Austin, W. E., Ramsey, C. B., Grootes, P. M., Hughen, K. A., Kromer, B., Reimer, P. J., Adkins, J. F., Burke, A., Cook, M. S., Olsen, J., and Skinner, L. C.: Marine20 - the marine radiocarbon age calibration curve (0 - 55,000 cal BP), simulated data for IntCal20, https://doi.org/10.1594/PANGAEA.914500, 2020.

Heaton, T. J., Butzin, M., Bard, E., Bronk Ramsey, C., Hughen, K. A., Köhler, P., & Reimer, P. J.: MARINE RADIOCARBON CALIBRATION IN POLAR REGIONS: A SIMPLE APPROXIMATE APPROACH USING MARINE20. Radiocarbon, 65(4), 848–875. doi:10.1017/RDC.2023.42. 2023.

Hemer, M. A. and Harris, P. T.: Sediment core from beneath the Amery Ice Shelf, East Antarctica, suggests mid-Holocene ice-shelf retreat, Geol, 31, 127, https://doi.org/10.1130/0091-7613(2003)031<0127:SCFBTA>2.0.CO;2, 2003.

Hillenbrand, C.-D., Larter, R. D., Dowdeswell, J. A., Ehrmann, W., Ó Cofaigh, C., Benetti, S., Graham, A. G. C., and Grobe, H.: The sedimentary legacy of a palaeo-ice stream on the shelf of the southern Bellingshausen Sea: Clues to West Antarctic glacial history during the Late Quaternary, QSR, 29, 2741–2763, https://doi.org/10.1016/j.quascirev.2010.06.028, 2010.

Hillenbrand, C.-D., Bentley, M. J., Stolldorf, T. D., Hein, A. S., Kuhn, G., Graham, A. G. C., Fogwill, C. J., Kristoffersen, Y., Smith, James. A., Anderson, J. B., Larter, R. D., Melles, M., Hodgson, D. A., Mulvaney, R., and Sugden, D. E.: Reconstruction of changes in the Weddell Sea sector of the Antarctic Ice Sheet since the Last Glacial Maximum, QSR, 100, 111–136, https://doi.org/10.1016/j.quascirev.2013.07.020, 2014.

Hodgson, D. A., Graham, A. G. C., Roberts, S. J., Bentley, M. J., Cofaigh, C. Ó., Verleyen, E., Vyverman, W., Jomelli, V., Favier, V., Brunstein, D., Verfaillie, D., Colhoun, E. A., Saunders, K. M., Selkirk, P. M., Mackintosh, A., Hedding, D. W.,

Nel, W., Hall, K., McGlone, M. S., Van Der Putten, N., Dickens, W. A., and Smith, J. A.: Terrestrial and submarine evidence for the extent and timing of the Last Glacial Maximum and the onset of deglaciation on the maritime-Antarctic and sub-Antarctic islands, QSR, 100, 137–158, https://doi.org/10.1016/j.quascirev.2013.12.001, 2014.

Ingolfsson O, Hjort C, Berkman PA, Bjorck S, Colhoun E, Goodwin ID, Hall B, Hirakawa K, Melles M, Moller P, Prentice ML: Antarctic glacial history since the Last Glacial Maximum: an overview of the record on land. Antarct Sci 10:326–344. 1998.

Jakobsson, M., Anderson, J. B., Nitsche, F. O., Gyllencreutz, R., Kirshner, A. E., Kirchner, N., O'Regan, M., Mohammad, R., and Eriksson, B.: Ice sheet retreat dynamics inferred from glacial morphology of the central Pine Island Bay Trough, West Antarctica, QSR, 38, 1–10, https://doi.org/10.1016/j.quascirev.2011.12.017, 2012.

Jamieson, S. S. R., Stokes, C. R., Livingstone, S. J., Vieli, A., Ó Cofaigh, C., Hillenbrand, C.-D., and Spagnolo, M.: Subglacial processes on an Antarctic ice stream bed. 2: Can modelled ice dynamics explain the morphology of mega-scale glacial lineations?, J. Glaciol., 62, 285–298, https://doi.org/10.1017/jog.2016.19, 2016.

Kattein, L., Höhn, M., Grotheer, H., Gentz, T., Mollenhauer, G.: Introducing a Ramped Pyrolysis/Oxidation-$^{14}CO_2$-analysis system operated with mobile molecular sieve traps, submitted to Limnology & Oceanography: Methods, 2026.

Klages, J. P., Kuhn, G., Hillenbrand, C.-D., Graham, A. G. C., Smith, J. A., Larter, R. D., and Gohl, K.: First geomorphological record and glacial history of an inter-ice stream ridge on the West Antarctic continental shelf, Quaternary Science Reviews, 61, 47–61, https://doi.org/10.1016/j.quascirev.2012.11.007, 2013.

Klages, J. P., Kuhn, G., Hillenbrand, C.-D., Graham, A. G. C., Smith, J. A., Larter, R. D., Gohl, K., and Wacker, L.: Retreat of the West Antarctic Ice Sheet from the western Amundsen Sea shelf at a pre- or early LGM stage, QSR, 91, 1–15, https://doi.org/10.1016/j.quascirev.2014.02.017, 2014.

Klages, J. P., Kuhn, G., Graham, A. G. C., Hillenbrand, C.-D., Smith, J. A., Nitsche, F. O., Larter, R. D., and Gohl, K.: Palaeo-ice stream pathways and retreat style in the easternmost Amundsen Sea Embayment, West Antarctica, revealed by combined multibeam bathymetric and seismic data, Geomorphology, 245, 207–222, https://doi.org/10.1016/j.geomorph.2015.05.020, 2015.

Klages, J. P., Kuhn, G., Hillenbrand, C.-D., Smith, J. A., Graham, A. G. C., Nitsche, F. O., Frederichs, T., Jernas, P. E., Gohl, K., and Wacker, L.: Limited grounding-line advance onto the West Antarctic continental shelf in the easternmost Amundsen Sea Embayment during the last glacial period, PLoS ONE, 12, e0181593, https://doi.org/10.1371/journal.pone.0181593, 2017.

Kusahara, K., Hasumi, H., Fraser, A. D., Aoki, S., Shimada, K., Williams, G. D., Massom, R., and Tamura, T.: Modeling Ocean–Cryosphere Interactions off Adélie and George V Land, East Antarctica, J. Climate, 30, 163–188, https://doi.org/10.1175/JCLI-D-15-0808.1, 2017.

Lanham, J., Mazloff, M., Naveira Garabato, A. C., Siegert, M., and Mashayek, A.: Seasonal regimes of warm Circumpolar Deep Water intrusion toward Antarctic ice shelves, Commun Earth Environ, 6, 168, https://doi.org/10.1038/s43247-025-02091-w, 2025.

Larter, R. D., Anderson, J. B., Graham, A. G. C., Gohl, K., Hillenbrand, C.-D., Jakobsson, M., Johnson, J. S., Kuhn, G., Nitsche, F. O., Smith, J. A., Witus, A. E., Bentley, M. J., Dowdeswell, J. A., Ehrmann, W., Klages, J. P., Lindow, J., Cofaigh, C. Ó., and Spiegel, C.: Reconstruction of changes in the Amundsen Sea and Bellingshausen Sea sector of the West Antarctic Ice Sheet since the Last Glacial Maximum, QSR, 100, 55–86, https://doi.org/10.1016/j.quascirev.2013.10.016, 2014.

Leventer, A., Domack, E., Dunbar, R., Pike, J., Stickley, C., Maddison, E., Brachfeld, S., Manley, P., and McClennen, C.: Marine sediment record from the East Antarctic margin reveals dynamics of ice sheet recession, Gsa Today, 16, 4, https://doi.org/10.1130/GSAT01612A.1, 2006.

Livingstone, S. J., Ó Cofaigh, C., Hogan, K. A., and Dowdeswell, J. A.: Submarine glacial-landform distribution along an Antarctic Peninsula palaeo-ice stream: a shelf–slope transect through the Marguerite Trough system (66–70° S), Memoirs, 46, 485–492, https://doi.org/10.1144/M46.180, 2016a.

Livingstone, S. J., Stokes, C. R., Ó Cofaigh, C., Hillenbrand, C.-D., Vieli, A., Jamieson, S. S. R., Spagnolo, M., and Dowdeswell, J. A.: Subglacial processes on an Antarctic ice stream bed. 1: Sediment transport and bedform genesis inferred from marine geophysical data, J. Glaciol., 62, 270–284, https://doi.org/10.1017/jog.2016.18, 2016b.

Mackintosh, A., White, D., Fink, D., Gore, D. B., Pickard, J., and Fanning, P. C.: Exposure ages from mountain dipsticks in Mac. Robertson Land, East Antarctica, indicate little change in ice-sheet thickness since the Last Glacial Maximum, Geol, 35, 551, https://doi.org/10.1130/G23503A.1, 2007.

Mackintosh, A., Golledge, N., Domack, E., Dunbar, R., Leventer, A., White, D., Pollard, D., DeConto, R., Fink, D., Zwartz, D., Gore, D., and Lavoie, C.: Retreat of the East Antarctic ice sheet during the last glacial termination, Nat. Geosci, 4, 195–202, https://doi.org/10.1038/ngeo1061, 2011.

Mackintosh, A. N., Verleyen, E., O'Brien, P. E., White, D. A., Jones, R. S., McKay, R., Dunbar, R., Gore, D. B., Fink, D., Post, A. L., Miura, H., Leventer, A., Goodwin, I., Hodgson, D. A., Lilly, K., Crosta, X., Golledge, N. R., Wagner, B., Berg, S., Van Ommen, T., Zwartz, D., Roberts, S. J., Vyverman, W., and Masse, G.: Retreat history of the East Antarctic Ice Sheet since the Last Glacial Maximum, QSR, 100, 10–30, https://doi.org/10.1016/j.quascirev.2013.07.024, 2014.

Majewski, W., Prothro, L. O., Simkins, L. M., Demianiuk, E. J., and Anderson, J. B.: Foraminiferal Patterns in Deglacial Sediment in the Western Ross Sea, Antarctica: Life Near Grounding Lines, Paleoceanog and Paleoclimatol, 35, e2019PA003716, https://doi.org/10.1029/2019PA003716, 2020.

Matsuoka, K., Skoglund, A., Roth, G., De Pomereu, J., Griffiths, H., Headland, R., Herried, B., Katsumata, K., Le Brocq, A., Licht, K., Morgan, F., Neff, P. D., Ritz, C., Scheinert, M., Tamura, T., Van De Putte, A., Van Den Broeke, M., Von Deschwanden, A., Deschamps-Berger, C., Van Liefferinge, B., Tronstad, S., and Melvær, Y.: Quantarctica, an integrated mapping environment for Antarctica, the Southern Ocean, and sub-Antarctic islands, Environ. Model.Softw, 140, 105015, https://doi.org/10.1016/j.envsoft.2021.105015, 2021.

Mawbey, E. M., Smith, J. A., Hillenbrand, C.-D., Hendry, K. R., McClymont, E. L., Greaves, M. J., Klages, J. P., Kuhn, G., Radionovskaya, S., Spencer-Jones, C. L., Larter, R. D., Wellner, J. S., and Dutrieux, P.: Ocean heat forced West Antarctic

Ice Sheet retreat after the Last Glacial Maximum, Nat Commun, 17, 2079, https://doi.org/10.1038/s41467-026-68949-5, 2026.

Mizuta, G., Ohshima, K. I., Takatsuka, T., Kitade, Y., Fujii, M., Nakayama, Y., and Ikehara, M.: Circulation and production of Cape Darnley Bottom Water on the continental slope off the Cape Darnley polynya, East Antarctica, Deep Sea Research Part I: ORP, 211, 104362, https://doi.org/10.1016/j.dsr.2024.104362, 2024.

Mollenhauer, G., Grotheer, H., Gentz, T., Bonk, E., and Hefter, J.: Standard operation procedures and performance of the MICADAS radiocarbon laboratory at Alfred Wegener Institute (AWI), Germany, Nuclear Instruments and Methods in Physics Research Section B: Beam Interactions with Materials and Atoms, 496, 45–51, https://doi.org/10.1016/j.nimb.2021.03.016, 2021.

Morlighem, M., Rignot, E., Binder, T., Blankenship, D., Drews, R., Eagles, G., Eisen, O., Ferraccioli, F., Forsberg, R., Fretwell, P., Goel, V., Greenbaum, J. S., Gudmundsson, H., Guo, J., Helm, V., Hofstede, C., Howat, I., Humbert, A., Jokat, W., Karlsson, N. B., Lee, W. S., Matsuoka, K., Millan, R., Mouginot, J., Paden, J., Pattyn, F., Roberts, J., Rosier, S., Ruppel, A., Seroussi, H., Smith, E. C., Steinhage, D., Sun, B., Broeke, M. R. V. D., Ommen, T. D. V., Wessem, M. V., and Young, D. A.: Deep glacial troughs and stabilizing ridges unveiled beneath the margins of the Antarctic ice sheet, Nat. Geosci., 13, 132–137, https://doi.org/10.1038/s41561-019-0510-8, 2020.

Nicola, L., Reese, R., Kreuzer, M., Albrecht, T., and Winkelmann, R.: Bathymetry-constrained warm-mode melt estimates derived from analysing oceanic gateways in Antarctica, The Cryosphere, 19, 2263–2287, https://doi.org/10.5194/tc-19-2263-2025, 2025.

Ó Cofaigh, C., Evans, J., Dowdeswell, J. A., and Larter, R. D.: Till characteristics, genesis and transport beneath Antarctic paleo-ice streams, J. Geophys. Res., 112, 2006JF000606, https://doi.org/10.1029/2006JF000606, 2007.

Ó Cofaigh, C., Davies, B. J., Livingstone, S. J., Smith, J. A., Johnson, J. S., Hocking, E. P., Hodgson, D. A., Anderson, J. B., Bentley, M. J., Canals, M., Domack, E., Dowdeswell, J. A., Evans, J., Glasser, N. F., Hillenbrand, C.-D., Larter, R. D., Roberts, S. J., and Simms, A. R.: Reconstruction of ice-sheet changes in the Antarctic Peninsula since the Last Glacial Maximum, QSR, 100, 87–110, https://doi.org/10.1016/j.quascirev.2014.06.023, 2014.

Ohshima, K. I., Fukamachi, Y., Williams, G. D., Nihashi, S., Roquet, F., Kitade, Y., Tamura, T., Hirano, D., Herraiz-Borreguero, L., Field, I., Hindell, M., Aoki, S., and Wakatsuchi, M.: Antarctic Bottom Water production by intense sea-ice formation in the Cape Darnley polynya, Nat. Geosci, 6, 235–240, https://doi.org/10.1038/ngeo1738, 2013.

Pedro, J. B., Bostock, H. C., Bitz, C. M., He, F., Vandergoes, M. J., Steig, E. J., Chase, B. M., Krause, C. E., Rasmussen, S. O., Markle, B. R., and Cortese, G.: The spatial extent and dynamics of the Antarctic Cold Reversal, Nat. Geosci, 9, 51–55, https://doi.org/10.1038/ngeo2580, 2016.

Peltier, W. R. & Fairbanks, R. G. : Global glacial ice volume and Last Glacial Maximum duration from an extended Barbados sea level record. QSR 25, 3322–3337. https://doi.org/10.1016/j.quascirev.2006.04.010, 2006.

Pritchard, H. D., Fretwell, P. T., Fremand, A. C., Bodart, J. A., Kirkham, J. D., Aitken, A., Bamber, J., Bell, R., Bianchi, C., Bingham, R. G., Blankenship, D. D., Casassa, G., Christianson, K., Conway, H., Corr, H. F. J., Cui, X., Damaske, D., Damm,

V., Dorschel, B., Drews, R., Eagles, G., Eisen, O., Eisermann, H., Ferraccioli, F., Field, E., Forsberg, R., Franke, S., Goel, V., Gogineni, S. P., Greenbaum, J., Hills, B., Hindmarsh, R. C. A., Hoffman, A. O., Holschuh, N., Holt, J. W., Humbert, A., Jacobel, R. W., Jansen, D., Jenkins, A., Jokat, W., Jong, L., Jordan, T. A., King, E. C., Kohler, J., Krabill, W., Maton, J., Gillespie, M. K., Langley, K., Lee, J., Leitchenkov, G., Leuschen, C., Luyendyk, B., MacGregor, J. A., MacKie, E., Moholdt, G., Matsuoka, K., Morlighem, M., Mouginot, J., Nitsche, F. O., Nost, O. A., Paden, J., Pattyn, F., Popov, S., Rignot, E., Rippin, D. M., Rivera, A., Roberts, J. L., Ross, N., Ruppel, A., Schroeder, D. M., Siegert, M. J., Smith, A. M., Steinhage, D., Studinger, M., Sun, B., Tabacco, I., Tinto, K. J., Urbini, S., Vaughan, D. G., Wilson, D. S., Young, D. A., and Zirizzotti, A.: Bedmap3 updated ice bed, surface and thickness gridded datasets for Antarctica, Sci Data, 12, 414, https://doi.org/10.1038/s41597-025-04672-y, 2025.

Reinardy, B. T. I., Hiemstra, J. F., Murray, T., Hillenbrand, C.-D., and Larter, R. D.: Till genesis at the bed of an Antarctic Peninsula palaeo-ice stream as indicated by micromorphological analysis: Till genesis at the bed of an Antarctic Peninsula palaeo-ice stream, Boreas, 40, 498–517, https://doi.org/10.1111/j.1502-3885.2010.00199.x, 2011.

Rignot, E., Mouginot, J., and Scheuchl, B.: Ice Flow of the Antarctic Ice Sheet, Sci., 333, 1427–1430, https://doi.org/10.1126/science.1208336, 2011.

Rignot, E., Mouginot, J., Scheuchl, B., Van Den Broeke, M., Van Wessem, M. J., and Morlighem, M.: Four decades of Antarctic Ice Sheet mass balance from 1979–2017, Proc. Natl. Acad. Sci. U.S.A., 116, 1095–1103, https://doi.org/10.1073/pnas.1812883116, 2019.

Silvano, A., Rintoul, S., and Herraiz-Borreguero, L.: Ocean-Ice Shelf Interaction in East Antarctica, Oceanog., 29, 130–143, https://doi.org/10.5670/oceanog.2016.105, 2016.

Sedwick, P. N., Harris, P. T., Robertson, L. G., McMurtry, G. M., Cremer, M. D., and Robinson, P.: Holocene sediment records from the continental shelf of Mac. Robertson Land, East Antarctica, Paleoceanography, 16, 212–225, https://doi.org/10.1029/2000PA000504, 2001.

Schoof, C.: Ice sheet grounding line dynamics: Steady states, stability, and hysteresis, J. Geophys. Res., 112, 2006JF000664, https://doi.org/10.1029/2006JF000664, 2007.

Simkins, L. M., Greenwood, S. L., and Anderson, J. B.: Diagnosing ice sheet grounding line stability from landform morphology, The Cryosphere, 12, 2707–2726, https://doi.org/10.5194/tc-12-2707-2018, 2018.

Smith, J. A., Graham, A. G. C., Post, A. L., Hillenbrand, C.-D., Bart, P. J., and Powell, R. D.: The marine geological imprint of Antarctic ice shelves, Nat Commun, 10, 5635, https://doi.org/10.1038/s41467-019-13496-5, 2019.

Schmidt, C., Morrison, A. K., and England, M. H.: Wind– and Sea-Ice–Driven Interannual Variability of Antarctic Bottom Water Formation, JGR Oceans, 128, e2023JC019774, https://doi.org/10.1029/2023JC019774, 2023.

Stuiver, M., and Reimer, P.J.: CALIB rev. 8, Radiocarb.,35, 215-230. Radiocarb.,35, 215-230. http://calib.org/calib/,1993.

The IMBIE team: Mass balance of the Antarctic Ice Sheet from 1992 to 2017, Nat., 558, 219–222, https://doi.org/10.1038/s41586-018-0179-y, 2018.

The RAISED Consortium. Bentley, M. J., Ó Cofaigh, C., Anderson, J. B., Conway, H., Davies, B., Graham, A. G. C., Hillenbrand, C.-D., Hodgson, D. A., Jamieson, S. S. R., Larter, R. D., Mackintosh, A., Smith, J. A., Verleyen, E., Ackert, R. P., Bart, P. J., Berg, S., Brunstein, D., Canals, M., Colhoun, E. A., Crosta, X., Dickens, W. A., Domack, E., Dowdeswell, J. A., Dunbar, R., Ehrmann, W., Evans, J., Favier, V., Fink, D., Fogwill, C. J., Glasser, N. F., Gohl, K., Golledge, N. R., Goodwin, I., Gore, D. B., Greenwood, S. L., Hall, B. L., Hall, K., Hedding, D. W., Hein, A. S., Hocking, E. P., Jakobsson, M., Johnson, J. S., Jomelli, V., Jones, R. S., Klages, J. P., Kristoffersen, Y., Kuhn, G., Leventer, A., Licht, K., Lilly, K., Lindow, J., Livingstone, S. J., Massé, G., McGlone, M. S., McKay, R. M., Melles, M., Miura, H., Mulvaney, R., Nel, W., Nitsche, F. O., O'Brien, P. E., Post, A. L., Roberts, S. J., Saunders, K. M., Selkirk, P. M., Simms, A. R., Spiegel, C., Stolldorf, T. D., Sugden, D. E., Van Der Putten, N., Van Ommen, T., Verfaillie, D., Vyverman, W., Wagner, B., White, D. A., Witus, A. E., and Zwartz, D.: A community-based geological reconstruction of Antarctic Ice Sheet deglaciation since the Last Glacial Maximum, QSR, 100, 1–9, https://doi.org/10.1016/j.quascirev.2014.06.025, 2014.

Thompson, A. F., Stewart, A. L., Spence, P., and Heywood, K. J.: The Antarctic Slope Current in a Changing Climate, Rev. Geophys, 56, 741–770, https://doi.org/10.1029/2018RG000624, 2018.

Tiedemann, R. and Müller, J.: The Expedition PS128 of the Research Vessel POLARSTERN to the Lazarew Sea, Riiser-Larsen Sea, Cosmonaut Sea, and Cooperation Sea in 2022. https://doi.org/10.57738/BzPM_0764_2022. 2022.

Wellner, J. S., Heroy, D. C., and Anderson, J. B.: The death mask of the antarctic ice sheet: Comparison of glacial geomorphic features across the continental shelf, Geomorphology, 75, 157–171, https://doi.org/10.1016/j.geomorph.2005.05.015, 2006.

Weertman, J.: Stability of the Junction of an Ice Sheet and an Ice Shelf, J. Glaciol., 13, 3–11, https://doi.org/10.3189/S0022143000023327, 1974.

Wong, A. P. S. and Riser, S. C.: Modified shelf water on the continental slope north of Mac Robertson Land, East Antarctica, Geophys. Res. Lett.., 40, 6186–6190, https://doi.org/10.1002/2013GL058125, 2013.